Phylogeographic reconstruction of the emergence and spread of Powassan virus in the northeastern United States

Chantal B.F. Vogels[1*@], Doug E. Brackney[2*], Alan P. Dupuis II[3,4*], Rebecca M. Robich[5*], Joseph R. Fauver[1,6], Anderson F. Brito[1,7], Scott C. Williams[8], John F. Anderson[2], Charles B. Lubelczyk[5], Rachel E. Lange[3,4], Melissa A. Prusinski[9], Laura D. Kramer[3,4], Jody L. Gangloff-Kaufmann[10], Laura B. Goodman[11], Guy Baele[12], Robert P. Smith[5#], Philip M. Armstrong[2#], Alexander T. Ciota[3,4#], Simon Dellicour[12,13#@], Nathan D. Grubaugh[1,14#@]

[1] Department of Epidemiology of Microbial Diseases, Yale School of Public Health, New Haven, CT, USA
[2] Center for Vector Biology and Zoonotic Diseases, Department of Entomology, The Connecticut Agricultural Experiment Station, New Haven, CT, USA
[3] The Arbovirus Laboratory, New York State Department of Health, Wadsworth Center, Slingerlands, NY, USA
[4] Department of Biomedical Sciences, State University of New York at Albany School of Public Health, Albany, NY, USA
[5] Vector-borne Disease Laboratory, MaineHealth Institute for Research, Scarborough, ME, USA.
[6] Department of Epidemiology, University of Nebraska Medical Center, Omaha, NE, USA
[7] Instituto Todos pela Saúde, São Paulo SP, Brazil
[8] Department of Environmental Science and Forestry, The Connecticut Agricultural Experiment Station, New Haven, CT, USA
[9] New York State Department of Health, Bureau of Communicable Disease Control, Albany, NY, USA
[10] Department of Entomology, Cornell University, Ithaca, NY, USA
[11] Department of Public and Ecosystem Health, Cornell University, Ithaca, NY, USA
[12] Department of Microbiology, Immunology and Transplantation, Rega Institute, KU Leuven, Leuven, Belgium
[13] Spatial Epidemiology Lab (SpELL), Université Libre de Bruxelles, Brussels, Belgium
[14] Department of Ecology and Evolutionary Biology, Yale University, New Haven, CT, USA

[*] Co-first authors
[#] Co-senior authors
[@] Co-corresponding authors

Abstract

Powassan virus is an emerging tick-borne virus of concern for public health, but very little is known about its transmission patterns and ecology. Here, we expanded the genomic dataset by sequencing 279 Powassan viruses isolated from *Ixodes scapularis* ticks from the northeastern United States. Our phylogenetic and phylogeographic reconstructions revealed that Powassan virus lineage II was likely introduced or emerged from a relict population in the Northeast between 1940-1975. Sequences strongly clustered by sampling location, suggesting a highly focal geographical distribution. Our analyses further indicated that Powassan virus lineage II emerged in the northeastern U.S. mostly following a south to north pattern, with a weighted lineage dispersal velocity of ~3 km/year. Since the emergence in the Northeast, we found an overall increase in the effective population size of Powassan virus lineage II, but with growth stagnating during recent years. The cascading effect of population expansion of white-tailed deer and *I. scapularis* populations likely facilitated the emergence of Powassan virus in the northeastern U.S.

Significance statement

Our work provides important fundamental insights in the local transmission dynamics of an emerging tick-borne pathogen of public health concern. Without the availability of vaccines or specific treatments, prevention of Powassan virus infection is dependent on education and control. We identified that Powassan virus is maintained in highly localized transmission foci that have been maintained for several years, without introductions of new virus clades. This provides both opportunities for better education about high risk areas and effective targeted control in Powassan virus foci with a long lasting impact.

Introduction

Reports of tick-borne diseases in the United States have been steadily rising, with more than 50,000 cases in 2019[1]. In that same year, a record number of 43 human cases of infection with an emerging tick-borne pathogen, Powassan virus (*Flaviviridae: Flavivirus*), were reported[2–5]. Powassan virus infection can cause severe neuroinvasive disease with long-lasting sequelae and high fatality rates in humans. Since its initial identification in 1958[6], incidence rates of Powassan neuroinvasive disease in humans have dramatically risen in the United States, particularly during recent years in the Northeast[7]. As Powassan virus infection is difficult to clinically diagnose[8] and most infections are asymptomatic[3], the reported cases are likely a vast underestimation of the true burden. The increasing number of human infections coupled with the lack of an effective vaccine or medicines, highlights the need to better understand local virus transmission patterns to guide targeted prevention and control measures.

Emergence of tick-borne diseases such as Lyme borreliosis, anaplasmosis, and babesiosis are associated with the spread of *Ixodes scapularis* ticks following expansion of suitable habitats[9] and the reintroduction of their primary adult stage hosts, white-tailed deer (*Odocoileus virginianus*), into the northeastern United States[10,11]. Powassan virus consists of two genetically distinct lineages, of which lineage II, also thought to be primarily maintained by *I. scapularis* ticks and small mammals[12,13] followed a similar path[3–5]. However, very little is known about its ecology and transmission patterns. Genetic approaches, including phylogenetic and phylogeographic

inference, are powerful tools to understand patterns of pathogen transmission and spread. However, until recently there were only 23 near-complete Powassan virus genomes available from the United States. Thus, to inform future control efforts and mitigate public health risks, there is a critical need for new and innovative phylogeographic approaches to uncover how Powassan virus is being maintained in the Northeast and which factors facilitate or prevent its spread to other areas.

To investigate, we partnered with public health laboratories throughout the Northeast to sequence Powassan virus isolated from *I. scapularis* ticks in Connecticut, New York, and Maine. We sequenced samples collected in 2008-2019 from both historic endemic sites and from novel regions on the leading edge of expansion in the Northeast. With this expanded genomic dataset, we performed discrete and continuous phylogeographic analyses to answer important questions on the emergence and spread of Powassan virus lineage II, such as: (**1**) When did Powassan virus lineage II emerge in the Northeast? (**2**) How is Powassan virus lineage II locally maintained? (**3**) What are the patterns and velocity of spread? (**4**) Can increased transmission explain the recent increase in reported human cases? (**5**) What is the impact of environmental factors on the dispersal dynamics? Overall, our study provides important insights in the emergence and spread of Powassan virus in the northeastern United States. Our findings help to better identify potential high-risk areas for exposure, which will in turn help to direct future control efforts.

Results

Powassan virus phylogeny

Powassan virus consists of two genetically and ecologically distinct lineages (lineage I and II; **Fig. 1**). Prior to this study, there were 23 near-complete Powassan virus genome sequences publicly available from the United States. In this study, we sequenced an additional 279 Powassan viruses (2 belonging to lineage I, and 277 belonging to lineage II) from positive tick pools identified by public health laboratories in Connecticut, New York, and Maine from 2008-2019 (**Supplementary Tables 1-3**). We created Nextstrain pages to visualize the Powassan genomic data with builds for all available genomes[14], and a more specific build for genomes available from the northeastern U.S.[15]. Publicly available lineage I sequences were available from Russia, Canada (initial case in North America), and the United States, but Powassan virus lineage I had not been reported from the United States since the late 1970s[16,17]. As part of this study, we sequenced two lineage I genomes detected in *I. scapularis* ticks in 2019 from New York. Later, we sequenced two additional lineage I genomes detected in *I. cookei* (2020) and *Dermacentor variabilis* (2021) also from New York[18]. Identification of Powassan virus lineage I in various tick species highlights how increased virus genomic surveillance can help to expand our knowledge of virus ecology.

Almost all of the more recent Powassan viruses detected from the US, including what we sequenced for this study, belong to lineage II. Powassan virus lineage II, also referred to as “deer tick virus”, consists of two geographically separated clades comprising viruses from the Midwest and the Northeast (**Fig. 1**). Powassan virus lineage II is the most prevalent in the Northeast, and we first carefully assessed the presence of temporal signal in these data. While the determination coefficient of the root-to-tip regression performed with TempEst[19] is relatively small (R^2 = 0.23; **Fig. 1**), we find very strong evidence in favor of temporal signal in the data set

using a recently developed Bayesian method[20] (log Bayes factor = 41.8[21]), enabling the use of molecular clocks to estimate time-calibrated phylogenies. As part of this analysis, we find that an uncorrelated relaxed clock with an underlying lognormal distribution provides a better model fit to the data compared to a strict clock model (**Table 1**). We estimate that the evolutionary rate of this clade is 8.25×10^{-5} substitutions/site/year (95% highest posterior density [HPD] interval: $8.23\text{-}10.46\times10^{-5}$]). Our estimate is higher than previous estimated evolutionary rates for all Powassan viruses (3.3×10^{-5})[22], and than previous estimates based on envelope (2.2×10^{-4})[5] and NS5 coding sequences ($3.9\times10^{-5}\text{-}5.4\times10^{-5}$)[5,23], likely a reflection of the recent emergence of lineage II in the region. Our work increased the number of publicly available Powassan virus lineage II sequences by more than ten-fold, enabling us to better understand the patterns of emergence and spread in the northeastern United States.

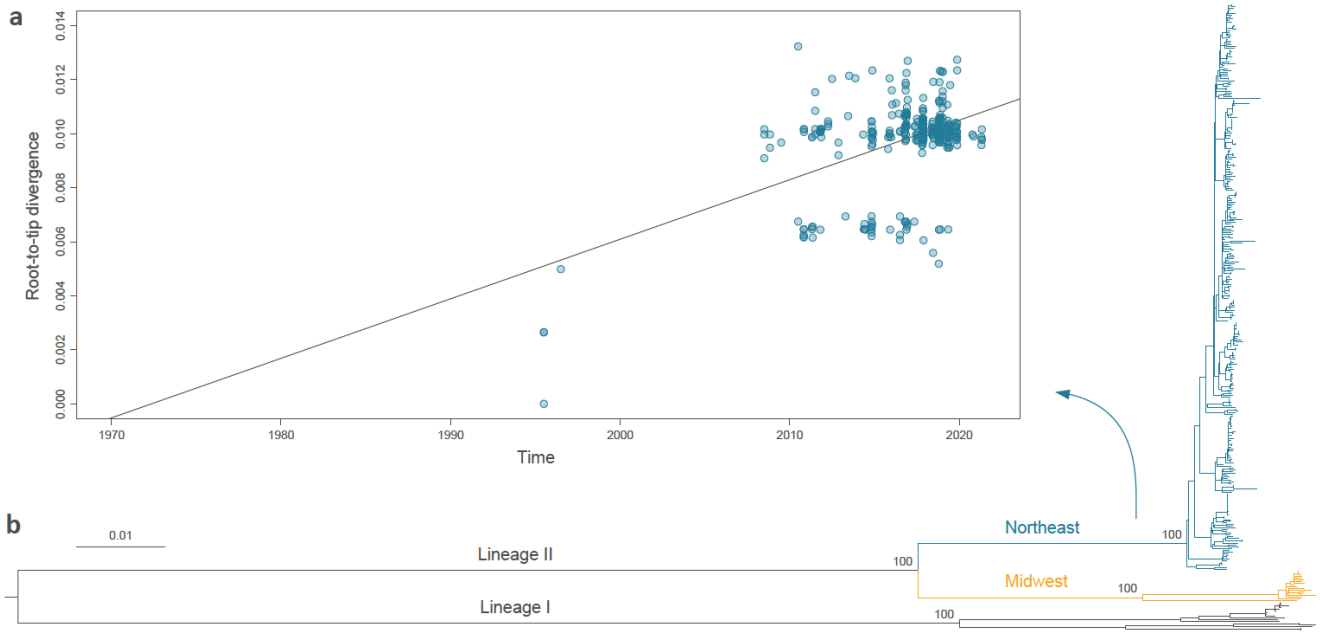

Fig. 1: Phylogenetic analysis of Powassan virus lineages. (a) Root-to-tip regression performed to assess the temporal signal within the Northeast clade (determination coefficient R^2 from the linear regression = 0.23). **(b)** Maximum likelihood tree was obtained from the phylogenetic analysis of publicly available Powassan virus genomes from the United States, Canada, and Russia. Powassan virus lineage II consists of two geographically separated clades in the Northeast and Midwest. Bootstraps support values (based on 1,000 replicates) are provided for the main internal nodes of the tree.

Emergence in the Northeast

The emergence of Powassan virus lineage II into the Northeast US likely followed the re-emergence of *I. scapularis* ticks, its primary vector, into the region. *Ixodes scapularis* originally colonized the Northeast thousands of years ago[24,25]; however, deforestation and restriction of white-tailed deer populations (primary reproductive host for adult *I. scapularis* ticks) during the 1800s greatly reduced *I. scapularis* populations in the Northeast[10,26]. Reforestation and increasing white-tailed deer populations during the mid-1900s then led to a re-emergence of *I. scapularis*[10,27,28].

Our expanded Powassan virus genomic data enabled us to reconstruct the dispersal history of Powassan virus lineage II in the Northeastern US (**Fig. 2a**). Our discrete phylogeographic analysis estimates that the time to the most recent common ancestor (tMRCA) for the Northeast Powassan virus lineage II clade is between 1940.3-1974.7 (95% HPD interval; mean 1957.9). This

means that lineage II emerged in the Northeast by at least this time period, corresponding to the re-emergence of *I. scapularis* ticks.

Distinct transmission foci

Like tick-borne encephalitis virus in Europe[29,30], Powassan virus is hypothesized to be primarily maintained within strict foci[31,32], meaning that the virus does not routinely migrate between locations. To test this hypothesis, we examined our discrete phylogeographic reconstruction of Powassan virus lineage II in the Northeast (**Fig. 2**). We found that sequences strongly cluster by location (**Fig. 2a**) with relatively few transition events over the past 20 years (**Fig. 2b**).

We further explored the spatial structure using a continuous phylogeographic approach (**Fig. 3**). These findings again highlight the highly focal distribution, with rare long-distance dispersal events leading to the establishment of new foci (**Fig. 3a-d**). These transmission foci are particularly clear in Connecticut, where, besides a single dispersal event between locations 1 (Westport) and 2 (Redding), we do not observe mixing between the 5 distinct locations (**Fig. 3d, inset**). For example, we estimate that the lineage II viruses sequenced in location 2 (Redding) have been separated from location 3 (Bridgeport) for ~33 years (95% HPD interval: 24-41), despite being less than 20 km apart.

We found the same pattern of isolated transmission foci with limited mixing for New York and Maine, albeit with more short distance dispersal events, particularly in New York (**Fig. 2b**, **Fig. 3d**). These differences may be explained due to differences in sampling (e.g. Powassan virus sequenced from ticks in New York included adults collected from deer), environmental barriers to spread (e.g. separation of Connecticut locations by rivers), or other ecological factors.

Overall, our data suggest that after the initial emergence of Powassan virus lineage II in the Northeast, migration between nearby and long-distance locations was relatively rare. This supports the hypothesis that Powassan virus is primarily maintained in highly localized transmission foci.

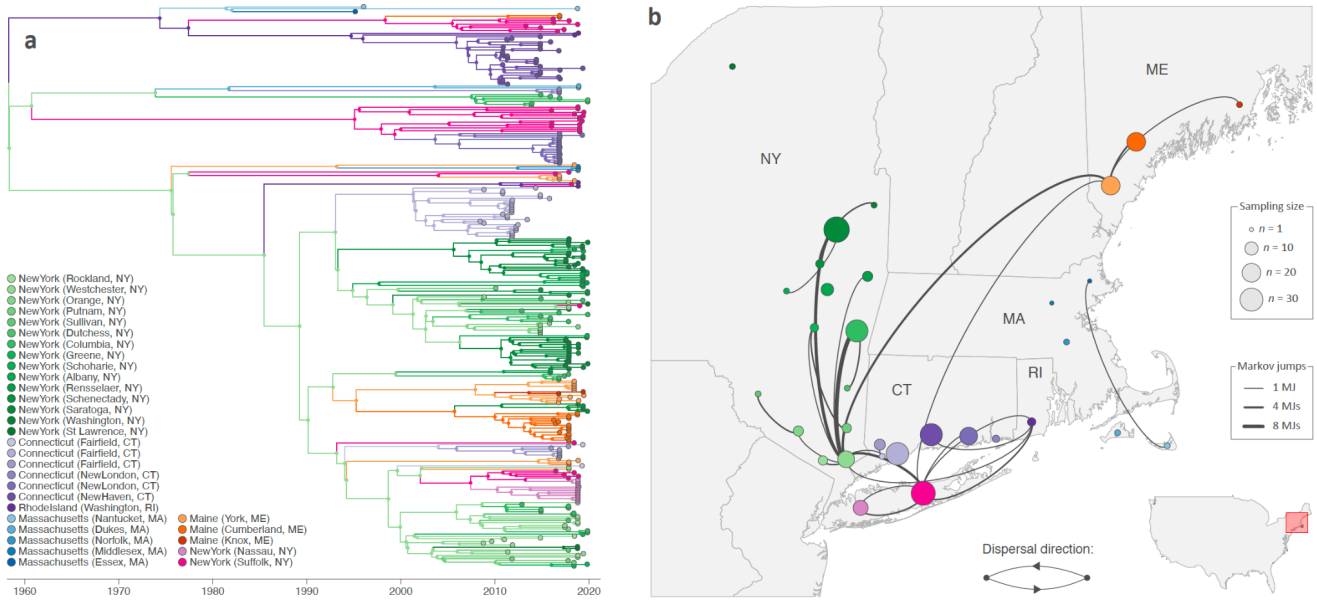

Fig. 2: Discrete phylogeographic analysis of the dispersal history of Powassan virus in the northeastern United States. (a) Maximum clade credibility (MCC) tree with branches colored according to the locations inferred at the

ancestral nodes. Tip nodes are colored according to their sampling location and are larger than internal nodes. **(b)** Sampling map and well-supported Markov jumps inferred by discrete phylogeographic inference. Sampling locations are displayed by dots with the size being proportional to the number of POWV genomic sequences sampled and included in our analyses. We only report Markov jumps associated with an adjusted Bayes factor support higher than 3, which corresponds to positive support according to the scale of interpretation as previously defined[21].

Dispersal history

While we have shown that Powassan virus lineage II in the Northeast is primarily restricted to strict foci, we wanted to better understand the patterns and velocity of spread. Our spatially explicit continuous phylogeographic analysis indicates that Powassan virus lineage II emerged in the Northeastern US mostly following a south to north pattern (**Fig. 3a-d**). We estimate that the virus first became established in southern New York and Connecticut by the late 1950s (1940.3-1974.7; **Fig. 3a**). This was followed by a few long-distance dispersal events to more northern regions, perhaps by infected ticks feeding on birds which can migrate over longer distances. We estimate that the virus finally became established in Maine by 1991 (95% HPD = [1968-2011]) through multiple introductions. Our estimates of the relatively recent dispersion of Powassan virus lineage II in the northern part of the Northeast suggest that the virus is likely still emerging in parts of North America, following the northward expansion of *I. scapularis*[33].

We then used our continuous phylogeographic results to estimate the dispersal velocity of Powassan virus lineage II through the Northeastern US. We estimated a weighted lineage dispersal velocity of ~3 km/year (95% HPD = [2.6-3.8]), which corresponds to a relatively slow dispersal capacity when compared to the estimates of the same metric obtained from the continuous phylogeographic analysis of other viruses (**Supplementary Table 4**). For instance, Powassan lineage II dispersed faster than the rodent-born Lassa virus in western Africa (~1 km/year)[34], but considerably slower than the mosquito-borne West Nile virus when it invaded North America (~165 km/year)[35]. Our dispersal velocity estimates can help us to track the current and future spread of the virus.

Population size

We next investigated if Powassan virus transmission has increased since its emergence in the Northeast, which could be a cause of the recent increase in reported human cases. We approached this by estimating the virus effective population size, which is influenced by changes in transmission intensity leading to the birth or death of virus lineages. Since the emergence in the Northeast, we found an overall increase in the effective population size of Powassan virus lineage II, but with growth stagnating since ~2005 (**Fig. 3e**). The latter could be a reflection of the virus becoming established across all of our study sites whereas the effective population size may still be increasing if we included additional sites in new emergence zones. Still, our data suggest that the increase in reported human cases in the region since 2010 (**Fig. 3f**) does not coincide with an increased virus effective population size (**Fig. 3e**). Thus, our findings do not support the hypothesis that the recent uptick in human cases is due to a significant increase in Powassan virus transmission; rather, it may be caused by an increase of human exposure to infected ticks.

As hypothesized as a significant factor for the timing of Powassan virus lineage II emergence in the Northeast, our overall estimates for the virus effective population size follow a similar trend as the population expansion of white-tailed deer in Connecticut and New York (**Fig. 3g**).

Reforestation in the Northeast has led to dramatic increases in the white-tailed deer populations, followed by population expansion of *I. scapularis*, which in turn has facilitated the emergence of tick-borne pathogens such as *Borrelia burgdorferi* and *Babesia microti*[27]. Our findings suggest that the cascading effect of population expansion of white-tailed deer and *I. scapularis* populations may also have facilitated the emergence of Powassan virus in the Northeast.

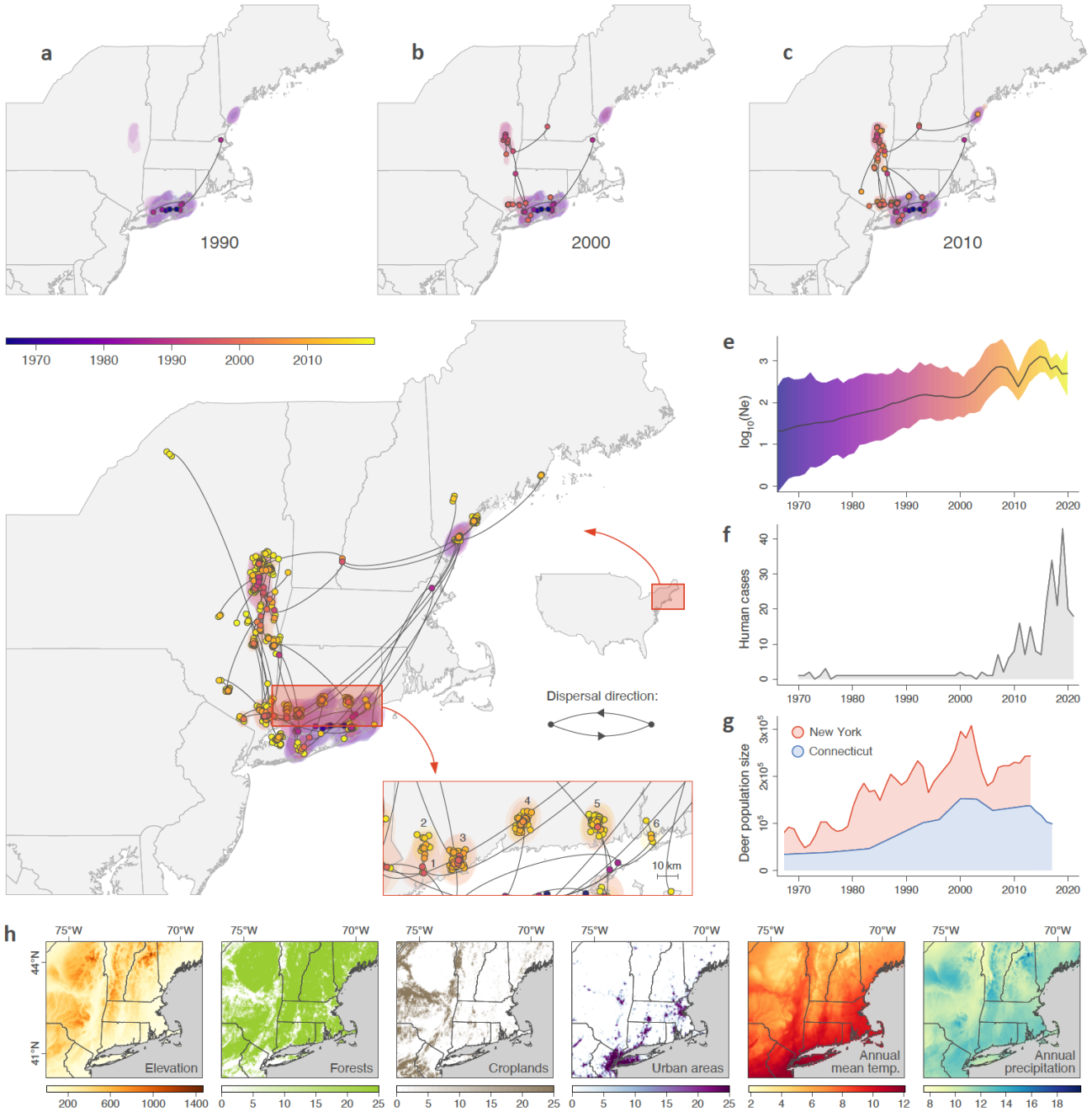

Fig. 3: Spatially-explicit phylogeographic analysis of the dispersal history of POWV in Northeastern USA. (a-d) Reconstruction of the dispersal history of POWV lineages inferred by a spatially-explicit phylogeographic analysis. We mapped branches of the maximum clade credibility (MCC) tree reported in Figure 2 and whose nodes, as well as associated 80% highest posterior density (HPD) regions, are colored according to their time of occurrence. **(e)** skygrid reconstruction of the evolution of the overall effective size of the viral population (Ne). **(f)** Evolution of the number of confirmed human cases. **(g)** Estimation of the white-tailed deer (*Odocoileus virginianus*) populations in the states of New York and Connecticut. **(h)** Environmental factors included in landscape phylogeographic analyses to test their impact on Powassan virus dispersal.

Impact of environmental factors on the dispersal dynamic

We exploited our spatially-explicit phylogeographic reconstruction to investigate the impact of environmental factors on the dispersal dynamic of Powassan lineage II. As detailed in the Methods section, we tested the association between a series of environmental factors (**Fig. 3h**) and the dispersal location[36] as well as velocity[37]. Our analyses revealed that inferred Powassan virus lineage II tended to avoid circulating in areas associated with relatively higher elevation (Bayes factor [BF] > 20; **Supplementary Table 5**). However, outcomes of our analysis are strongly influenced by the sampling effort and pattern, and therefore we are able to describe environmental conditions related to dispersal locations of inferred viral lineages, but we cannot draw conclusions on the actual impact of those conditions on the dispersal[36]. This observation could be related to higher abundance of *I. scapularis* at lower altitudes. Next, we investigated the impact of environmental factors on the dispersal velocity of Powassan virus lineage II. Our analyses did not highlight any environmental factor associated with the heterogeneity of Powassan lineage dispersal velocity across the study area (**Supplementary Table 6**). This means that none of the tested factors increased the correlation between dispersal duration and geographic distance, the latter thus remaining the main resistance factor to dispersal.

Discussion

Despite a rapid increase in the number of Powassan virus infections in humans over recent years, very little was known about the patterns of virus emergence and spread. By sequencing 279 Powassan virus genomes and using phylogenetic and phylogeographic approaches, we have uncovered the patterns of virus emergence, transmission, and spread in the northeastern U.S. Our analyses revealed that Powassan virus lineage II likely emerged in the Northeast around 1940-1975, following the population growth of white-tailed deer and expansion of *I. scapularis* tick populations[10,27]. Powassan virus lineage II is maintained in highly localized transmission foci, with few migration events between relatively nearby locations. Our continuous phylogeographic analysis revealed that Powassan virus lineage II likely emerged from southern Connecticut into more northern regions with a weighted lineage dispersal velocity of ~3 km/year. Although we found an overall upward trend in the virus effective population size over the last decades, the recent increase in reported human cases of Powassan virus infection does not coincide with a higher effective population size. This suggests that the recent uptick in human cases is likely not due to a significant increase in Powassan virus enzootic transmission, but it may rather be due to other factors such as increased human exposure to infected ticks as well as an increase in case recognition. Our findings provide important insights in the local emergence patterns and transmission dynamics of Powassan virus in the northeastern U.S. Insights into the highly localized transmission foci that sustain Powassan virus transmission across multiple years, will help to identify areas with high risk of spillover to the human population, which can be targeted for prevention education or control efforts.

Our reconstruction of the emergence of Powassan virus in the northeast follows similar patterns as the emergence reported for other tick-borne pathogens such as *Borrelia*, *Babesia*, and *Anaplasma*[38]. Similar to Powassan virus, these pathogens are maintained in transmission cycles involving *I. scapularis* as the main vector and white-footed mice (*Peromyscus leucopus*) as the main host. Introduction of these tick-borne pathogens in the northeastern United States follows the reforestation in the 20th century leading to rapid population expansions of both white-tailed

deer and *I. scapularis*[27,33]. Despite the similarities in emergence and ecology, other tick-borne pathogens seem to have more widespread distributions as compared to the highly focal distribution of Powassan virus. Previous studies on *Borrelia burgdorferi* reported high genetic diversity within local populations[39], lack of population genetic structure[24], and no strict genetic clustering by location within the Northeast[11]. This suggests that despite the similarities in ecology, *B. burgdorferi* and Powassan virus are maintained by different mechanisms.

To explain the highly focal distribution, we have formulated two main hypotheses on how Powassan virus lineage II may be maintained in strict transmission foci (**Fig. 4**). Our first hypothesis is that vertical transmission from adult to the next larval stage plays a minor role in the Powassan virus transmission cycle. Adult *I. scapularis* ticks preferentially feed on larger mammals, such as white-tailed deer, and we would expect more mixing of Powassan virus clades if infected adults travel across larger distances when feeding on deer, particularly during early years of emergence when deer habitats were less fragmented. Inefficient vertical transmission from adult to larvae would explain why adults and ticks may move, while Powassan virus foci remain local. Previous studies have provided evidence for vertical transmission of Powassan virus (i.e. one of six infected females transmitted Powassan virus to its progeny)[40], but it remains unclear what percentage of progeny within an egg batch becomes infected. Future studies can help to test this hypothesis by determining rates of vertical transmission in the laboratory, and determining infection rates of unfed larvae in the field.

Our second hypothesis is that backward transmission through life stages from nymphs to larvae is the main mechanism for Powassan virus maintenance (**Fig. 4**). Powassan virus clades better match the strong geographical structure of white-footed mice[41,42] and other small mammals that share the same habitat rather than the weak structure of *I. scapularis* ticks[25]. This suggests that Powassan virus is mostly maintained by local transmission cycles that include larvae and nymphs feeding on small mammals, and adult ticks and other animals that can travel long distances are primarily dead-ends, although sporadic long-distance dispersal events may happen. Backward transmission from nymphs to larvae may either occur through direct co-feeding transmission in the absence of systemic infection of the rodent host, as has been reported for tick-borne encephalitis virus[43,44], or through feeding on viremic hosts. To further investigate this hypothesis, we propose studies to determine the frequency of co-feeding between nymphs and larvae, to determine the size of transmission foci, and to perform comparative genetics between Powassan virus, *I. scapularis*, and small mammalian hosts, such as white-footed mice.

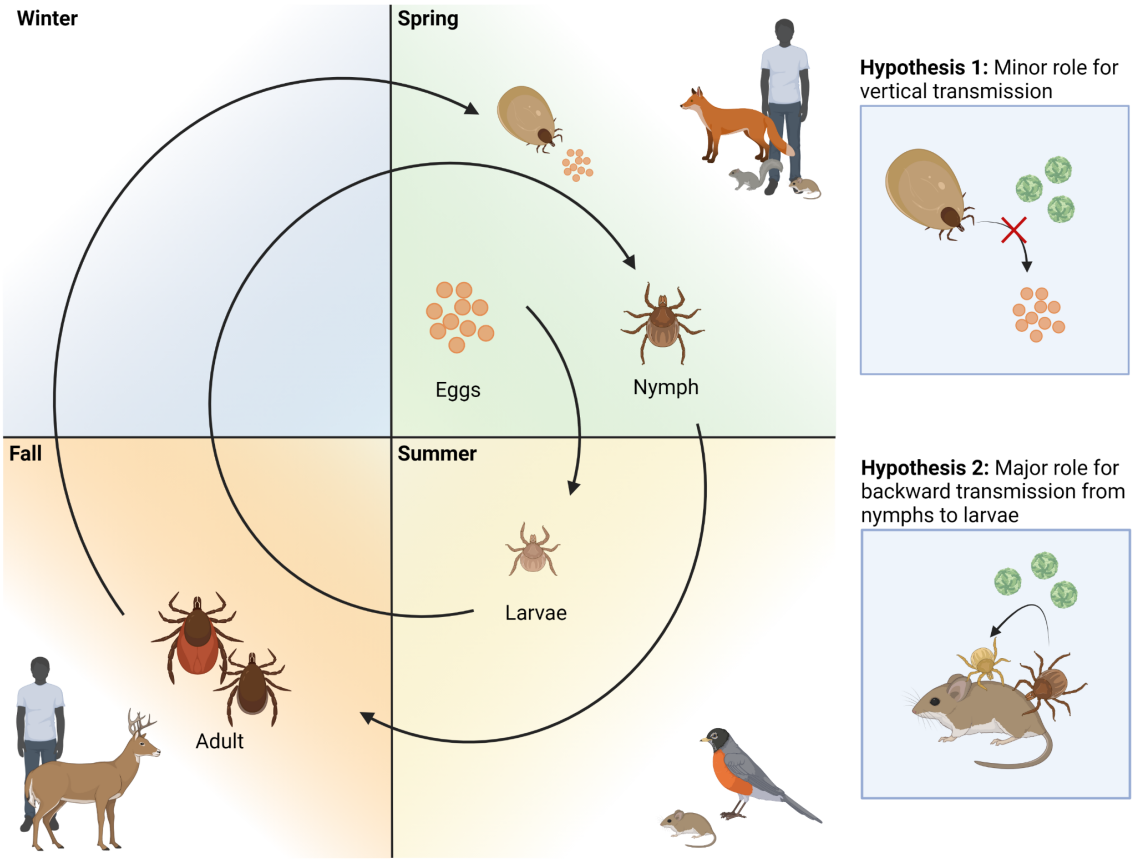

Fig. 4: *Ixodes scapularis* life cycle with proposed hypotheses that may explain the focal distribution of Powassan virus. Life cycle adapted from [38] and created with bioRender.com. Two hypotheses are proposed that may explain the focal distribution of Powassan virus.

Our study has several limitations. First, sampling strategy was not standardized across the northeastern United States nor was it standardized across time. Powassan virus surveillance activities are organized at the state level, and therefore there are differences in effort between states. For instance, samples sequenced from Connecticut and Maine were collected from the same sites during multiple years, whereas a much larger number of varying sites were sampled from year to year in New York. Sampling in New York also included tick collections from hunter-harvested deer, whereas sampling in Connecticut and Maine was exclusively done via drag sampling. Spatial heterogeneity in sampling effort will impact phylogeographic reconstructions, with unsampled locations being excluded from the reconstructed dispersal history, and undersampling of locations may lead to underestimation of the degree of connectivity between sites. Second, we attempted to include as many publicly available genomes in our analyses, but some genomes had to be excluded because they did not have complete metadata (e.g. missing collection date and location) or because they did not fit the molecular clock (e.g. Powassan sequences from human infections). Lastly, choice of molecular clock model may impact estimates for the evolutionary rate and the tMRCA. For example, when performing the analyses with a strict molecular clock model instead of a relaxed clock model, we get a lower estimated evolutionary rate of 3.80×10^{-5} substitutions/site/year (95% HPD = $2.60\text{-}5.57\times10^{-5}$) and an earlier tMRCA of 1882.8 (95% HPD = 1833.4-1936.9). This highlights the importance of molecular clock model choice based on best model fit and that we should be careful in our interpretation of the relaxed clock model estimates. Our estimates of emergence by the late 1950s should be interpreted as emergence by at least this time period, and not as an exact estimate of the emergence time.

Our study has important implications for our understanding of Powassan virus transmission dynamics and future control. Currently, no vaccines or specific treatments are available for Powassan virus infection, which leaves prevention of disease highly dependent on education and control. The identification of highly localized transmission foci provides both opportunities for better education of the general public about high risk areas and effective targeted control in Powassan virus hotspots. Eradication of Powassan virus in transmission foci that have been maintained for several years without introductions of new virus clades, will likely result in highly effective and long lasting control.

Methods

Sample collection

Tick collections, nucleic acid extraction, and Powassan virus screening were done at the Connecticut Agricultural Experiment Station (CAES), MaineHealth Institute for Research (MHIR), New York State Department of Health (NYSDOH), and Cornell University[31,45–48]. Briefly, the majority of ticks were collected by dragging a white cloth over the ground and low vegetation, and a smaller proportion were collected from vertebrate hosts (e.g. deer). All collected ticks were sorted by species, life stage, collection site and date before screening for pathogens. Individual or pooled ticks were homogenized and nucleic acid was extracted according to manufacturer's instructions (**Supplementary Table 1**). Powassan virus was detected by RT-qPCR or nanochip assays[31,45–48]. Samples collected from 2008 through 2016 in Connecticut were passaged once on BHK-21 cells before nucleic acid extraction.

Untargeted metagenomic Illumina sequencing

We initially used an untargeted metagenomic approach to sequence Powassan virus isolates which were passaged on cells at CAES. Our protocol is adapted from[49], and is openly available[50]. In brief, 10 µL of extracted nucleic acid was treated with DNase I (New England Biolabs, Ipswich, MA), followed by a clean up step using a ratio of 1.8:1 beads to sample. All clean up steps were done using MagBind TotalPure NGS magnetic beads (Omega Biotek, Norcross, GA) with automated protocols for the Kingfisher flex purification system (Thermo Fisher Scientific, Waltham, MA). First-strand cDNA was synthesized using SuperScript IV VILO (Thermo Fisher Scientific) and second-strand cDNA using *Escherichia coli* DNA ligase and polymerase (New England Biolabs), followed by a clean up step (1.8:1 beads to sample ratio). Libraries were prepared using the Nextera XT DNA library preparation kit for Illumina (Illumina, San Diego, CA), according to manufacturer's instructions but using less than the recommended reagent volumes[51]. Individual and pooled libraries were quantified using the 1x dsDNA HS assay kit on the Qubit 4 (Thermo Fisher Scientific) and size distribution was determined using the high sensitivity DNA kit on the Bioanalyzer 2100 (Agilent, Santa Clara, CA). Pooled libraries were sequenced on the Illumina NovaSeq (paired-end 150) at the Yale Center for Genome Analysis. PCR duplicates were removed, reads were aligned to the reference genome using Bowtie2, and consensus genomes were called at a minimum frequency threshold of 0.75 and minimum coverage of 10X using Geneious Prime 2020.0.4.

Targeted amplicon-based sequencing

Although we were able to successfully sequence Powassan virus from cell culture-passage samples using untargeted metagenomics, we developed an amplicon-based sequencing approach to improve coverage when sequencing from tick homogenates. We used an adapted protocol[52], using Nextera XT for library prep as developed for SARS-CoV-2 amplicon-based sequencing[53]. In brief, cDNA was synthesized from 10 µL of RNA using SuperScript IV VILO (Thermo Fisher Scientific). Two separate primer pools were prepared by mixing equal volumes of each primer with a concentration of 10 µM (**Supplementary Table 2**). The two primer pools were used to generate tiled amplicons using Q5 high-fidelity 2X master mix (New England Biolabs), followed by a clean up step and quantification using the Qubit. Amplicons were diluted to 1 ng/µL and combined for library prep as described above. Pooled libraries were quantified on Qubit and size distribution were determined on the bioanalyzer. Pooled libraries were sequenced on the Illumina NovaSeq (paired-end 150) at the Yale Center for Genome Analysis. Consensus genomes were generated at a minimum frequency threshold of 0.75 and minimum coverage of 10X using iVar version 1.2.3. All sequencing data is publicly available under BioProject PRJNA889421 and **Supplementary Table 3**.

Powassan virus phylogeny

We sequenced 279 Powassan virus genomes and estimated a maximum-likelihood tree using IQ-TREE version 1.6.12 with ultrafast bootstrap approximation (1,000 replicates)[54] to determine phylogenetic relationships between publicly available and newly sequenced Lineage I and II genomes.

Temporal signal assessment

To evaluate if our Powassan virus data set contains sufficient temporal signal and would permit time-calibrated analyses using molecular clock models (and hence constitutes a measurably evolving population), we performed a Bayesian Evaluation of Temporal Signal (BETS) analysis[20,55]. This analysis involves assessing the model fit to the data of both a strict clock and an uncorrelated relaxed clock with an underlying lognormal distribution, both with and without the sampling dates associated with the genomes in our data set (**Table 1**). We employed generalized stepping-stone sampling[56] to accurately estimate the log marginal likelihood of each of these four models. For each log marginal likelihood estimation, we ran an initial Markov chain of 500 million iterations, followed by 500 power posteriors that are explored during 1 million iterations, logging every 1000 iterations.

Table 1: Bayesian Evaluation of Temporal Signal analysis.

Clock model	Model fit
Strict clock + dates	-36575.48
Strict clock - dates	-36601.19
Relaxed clock + dates	-36512.57
Relaxed clock - dates	-36554.33

Discrete phylogeographic reconstruction

To investigate the dispersal history of POWV lineages in Northeastern America, we first conducted a discrete phylogeographic analysis using the Bayesian stochastic search variable selection (BSSVS) model[57] implemented in BEAST 1.10[58]. For this analysis, we considered each U.S. county of origin as a distinct location, except for the Connecticut area where each sampling site was considered as a distinct discrete location. We modeled the branch-specific evolutionary rates according to a relaxed molecular clock with an underlying log-normal distribution[59] and the nucleotide substitution process according to a GTR+Γ parameterisation[60]; and we specified a flexible skygrid model as the tree prior[61]. Three independent Markov chain Monte Carlo (MCMC) algorithms were run for 5×10^8 iterations and sampled every 10^5 iterations. Resulting posterior distributions were eventually combined after having discarded 10% of sampled trees in each of them. We used the program Tracer 1.7[62] for assessing the convergence and mixing properties, and that estimated sampling size (ESS) values associated with estimated parameters were all >200 after having combined the outputs of the three independent analyses. We then used the program TreeAnnotator 1.10[58] to obtain a maximum clade credibility (MCC) tree. We reported Markov jumps between discrete locations as estimated by the BSSVS analyses and supported by an adjusted Bayes factor (BF) values >3, which correspond to at least "positive" statistical support following the scale of interpretation defined by Kass & Raftery[21]. The adjusted BF support takes into account the relative abundance of samples by location[63] and is based on a tip labels swapping procedure similar to a tip date randomization that can be performed to test for temporal signal[64].

Continuous phylogeographic reconstruction

To reconstruct the dispersal history of POWV lineages in a spatially-explicit context, we performed a continuous phylogeographic analysis using the relaxed random walk (RRW) diffusion model [65,66] implemented in the software package BEAST 1.10[58], with a gamma distribution to model the among-branch heterogeneity in diffusion velocity. As for the discrete phylogeographic analysis, branch-specific evolutionary rates were modeled according to a relaxed molecular clock with an underlying log-normal distribution and the nucleotide substitution process according to a GTR+Γ parameterisation[60]; and we also specified a flexible skygrid model as the tree prior[61]. The Markov chain Monte-Carlo (MCMC) algorithm was run for 15×10^8 generations and sampled every 10^5 generations. We used the program Tracer 1.7 for assessing the convergence and mixing properties, and that estimated sampling size (ESS) values associated with estimated parameters were all >200, the program TreeAnnotator 1.10 to obtain a maximum clade credibility (MCC) tree, as well as the R package "seraphim" [67,68] to extract the spatiotemporal information embedded within posterior trees and to estimate the weighted lineage dispersal velocity, the latter being defined as follows:

$$v = \frac{\sum_{i=1}^{n} d_i}{\sum_{i=1}^{n} t_i}$$

where d_i and t_i are the geographic distance traveled by the phylogeny branch and the duration of that branch, respectively.

Landscape phylogeographic analyses

Landscape phylogeographic analyses aim at exploiting phylogeographic reconstructions to unravel the impact of environmental factors on the dispersal history and dynamic of viral lineages[69]. Specifically, we implemented two previously introduced analytical procedures to

investigate the impact of environmental factors on the dispersal location[36] and velocity[37] of POWV lineages. Both analytical procedures here rely on the comparison between inferred and randomized spatially-annotated trees, the latter sharing the time-scaled topology of the inferred trees but with phylogenetic branch positions that had been randomized across the study area. In practice, phylogenetic node positions were randomized within the study area, under the constraint that branch length (i.e. geographic distance connecting both branch nodes), branch duration, tree topology, and root position remained unchanged[67]. The purpose of these randomizations is thus to obtain spatially-annotated trees corresponding to the trees inferred by continuous phylogeography but along which we generated a new diffusion process that has been impacted by any environmental factor.

We first investigated whether POWV lineages tended to avoid or preferentially circulate within areas associated with particular environmental conditions. For this purpose, we extracted and subsequently averaged the environmental values at the tree node positions to obtain, for each environmental factor, a posterior distribution of mean environmental values at tree node positions. We then compared values obtained through inferred trees and their corresponding randomized trees using an approximated Bayes factor (BF) support[70]: BF = (p_e/(1-p_e))/(0.5/(1-0.5). To test if a particular environmental factor *e* tended to attract viral lineages, p_e was defined as the frequency at which the environmental values from inferred trees were greater than values from randomized trees; and to test if a particular environmental factor *e* tended to repulse viral lineages, p_e was defined as the frequency at which the environmental values from inferred trees were lower than values from randomized trees. We considered BF values > 20 and 3 < BF < 20 as strong and positive statistical supports, respectively[21].

Second, we investigated to what extent POWV lineage dispersal velocity was impacted by environmental factors acting as conductance or resistance factors. For each branch in the inferred and randomized trees we calculated an "environmental distance" using two path models: the least-cost path[71] and Circuitscape[72] algorithms, the latter accommodating uncertainty in the travel route. An environmental distance is calculated first from the raster of the environmental variable, and second from a uniform “null” raster whose cell values are all set to “1”. The environmental distance is a spatial distance that is weighted according to the values of the underlying environmental raster, and therefore constitutes a proxy for geographical distance when computed on the null raster. Each environmental variable was considered twice: once as a potential conductance factor that facilitates movement, and once as a potential resistance factor that impedes it. For each environmental variable, we also generated and tested several distinct rasters by transforming the original raster cell values with the following formula: $v_t = 1 + k(v_o/v_{max})$, where v_t and v_o are the transformed and original cell values, and v_{max} the maximum cell value recorded in the raster. The rescaling parameter *k* here allows the definition and testing of different strengths of raster cell conductance or resistance, relative to the conductance/resistance of a cell with a minimum value set to “1”, which corresponds to the “null” raster. For each environmental variable, we generated three distinct rasters using the following values for rescaling factor *k*: *k* = 10, 100, and 1000. For these analyses, we estimated the statistic *Q* defined as the difference between the coefficient of determinations obtained (i) when branch durations are regressed against the environmental distances computed on an environmental and (ii) when branch durations are regressed against the environmental distances computed on the null raster. We estimated a *Q* statistic for each environmental raster and each of the 1,000 trees sampled from the posterior distribution. An environmental factor was only considered as potentially explanatory if both its distribution of regression coefficients and its associated

distribution of *Q* values were positive[73], i.e. with at least 90% of positive values. In this case, the statistical support associated with the resulting *Q* distribution was compared with the corresponding null of distribution of *Q* values obtained when computing environmental distances for phylogenetic branches of randomized trees. Similar to the procedure used for the investigation of the impact of environmental factors on the dispersal locations of POWV lineages, the comparisons between inferred and randomized distributions of *Q* values was formalized by approximating a Bayes factor support[37].

Data availability

All data are included in this article, the supplementary files, and in BioProject PRJNA889421.

References

1. Centers for Disease Control and Prevention, National Center for Emerging and Zoonotic Infectious Diseases (NCEZID), Division of Vector-Borne Diseases (DVBD). Tickborne disease surveillance data summary. *CDC* https://www.cdc.gov/ticks/data-summary/index.html (2019).
2. ArboNET, Arboviral Diseases Branch, Centers for Disease Control and Prevention. Powassan virus neuroinvasive disease cases reported by year, 2008–2017. https://www.cdc.gov/powassan/statistics.html (2018).
3. Hermance, M. E. & Thangamani, S. Powassan Virus: An Emerging Arbovirus of Public Health Concern in North America. *Vector Borne Zoonotic Dis.* **17**, 453–462 (2017).
4. Ebel, G. D. Update on Powassan virus: emergence of a North American tick-borne flavivirus. *Annu. Rev. Entomol.* **55**, 95–110 (2010).
5. Pesko, K. N., Torres-Perez, F., Hjelle, B. L. & Ebel, G. D. Molecular epidemiology of Powassan virus in North America. *J. Gen. Virol.* **91**, 2698–2705 (2010).
6. McLean, D. M. & Donohue, W. L. Powassan virus: Isolation of virus from a fatal case of encephalitis. *Canadian Medical Association Journal* **80**, 708–711 (1959).
7. CDC. Powassan Virus Statistics & Maps. https://www.cdc.gov/powassan/statistics.html (2021).
8. Piantadosi, A. *et al.* Rapid Detection of Powassan Virus in a Patient With Encephalitis by Metagenomic Sequencing. *Clin. Infect. Dis.* **66**, 789–792 (2018).
9. Sonenshine, D. E. Range Expansion of Tick Disease Vectors in North America: Implications for Spread of Tick-Borne Disease. *Int. J. Environ. Res. Public Health* **15**, (2018).
10. Spielman, A., Wilson, M. L., Levine, J. F. & Piesman, J. Ecology of *Ixodes dammini*-borne human Babesiosis and Lyme disease. *Annual Review of Entomology* **30**, 439–460 (1985).
11. Hoen, A. G. *et al.* Phylogeography of *Borrelia burgdorferi* in the eastern United States reflects multiple independent Lyme disease emergence events. *Proc. Natl. Acad. Sci. U.S.A.* **106**, 15013–15018 (2009).
12. Ebel, G. D., Campbell, E. N., Goethert, H. K., Spielman, A. & Telford, S. R. Enzootic transmission of deer tick virus in New England and Wisconsin sites. *The American Journal of Tropical Medicine and Hygiene* **63**, 36–42 (2000).
13. Goethert, H. K., Mather, T. N., Johnson, R. W. & Telford, S. R., 3rd. Incrimination of shrews as a reservoir for Powassan virus. *Commun Biol* **4**, 1319 (2021).
14. Nextstrain build for Powassan virus. https://nextstrain.org/community/grubaughlab/powassan-genomics/All.
15. Nextstrain build for Powassan virus in the northeastern United States.

https://nextstrain.org/community/grubaughlab/powassan-genomics/NE.
16. CDC. Powassan Virus Isolated from a Patient with Encephalitis. *Morbidity and Mortality Weekly Report* **24**, 379 (1975).
17. Main, A. J., Carey, A. B. & Downs, W. G. Powassan virus in *Ixodes cookei* and *Mustelidae* in New England. *Journal of Wildlife Diseases* **15**, 585–591 (1979).
18. Hart, C. *et al.* First detection of Powassan Virus lineage I in field-collected Dermacentor variabilis from New York, USA. *medRxiv* 2022.03.01.22271704 (2022).
19. Rambaut, A., Lam, T. T., Max Carvalho, L. & Pybus, O. G. Exploring the temporal structure of heterochronous sequences using TempEst (formerly Path-O-Gen). *Virus Evol* **2**, vew007 (2016).
20. Duchene, S. *et al.* Bayesian Evaluation of Temporal Signal in Measurably Evolving Populations. *Mol. Biol. Evol.* **37**, 3363–3379 (2020).
21. Kass, R. E. & Raftery, A. E. Bayes Factors. *J. Am. Stat. Assoc.* **90**, 773–795 (1995).
22. Bondaryuk, A. N. *et al.* Phylogeography and Re-Evaluation of Evolutionary Rate of Powassan Virus Using Complete Genome Data. *Biology* **10**, (2021).
23. Subbotina, E. L. & Loktev, V. B. Molecular evolution of the tick-borne encephalitis and Powassan viruses. *Mol. Biol.* **46**, 75–84 (2012).
24. Humphrey, P. T., Caporale, D. A. & Brisson, D. Uncoordinated phylogeography of *Borrelia burgdorferi* and its tick vector, *Ixodes scapularis*. *Evolution* **64**, 2653–2663 (2010).
25. Walter, K. S., Carpi, G., Caccone, A. & Diuk-Wasser, M. A. Genomic insights into the ancient spread of Lyme disease across North America. *Nature Ecology & Evolution* **1**, 1569–1576 (2017).
26. Lee, X., Hardy, K., Johnson, D. H. & Paskewitz, S. M. Hunter-killed deer surveillance to assess changes in the prevalence and distribution of Ixodes scapularis (Acari: Ixodidae) in Wisconsin. *J. Med. Entomol.* **50**, 632–639 (2013).
27. Spielman, A. The emergence of Lyme disease and human babesiosis in a changing environment. *Ann. N. Y. Acad. Sci.* **740**, 146–156 (1994).
28. Eisen, R. J., Eisen, L. & Beard, C. B. County-Scale Distribution of Ixodes scapularis and Ixodes pacificus (Acari: Ixodidae) in the Continental United States. *J. Med. Entomol.* **53**, 349–386 (2016).
29. Randolph, S. E., Miklisová, D., Lysy, J., Rogers, D. J. & Labuda, M. Incidence from coincidence: patterns of tick infestations on rodents facilitate transmission of tick-borne encephalitis virus. *Parasitology* **118 (Pt 2)**, 177–186 (1999).
30. Labuda, M. & Randolph, S. E. Survival strategy of tick-borne encephalitis virus: cellular basis and environmental determinants. *Zentralbl. Bakteriol.* **289**, 513–524 (1999).
31. Anderson, J. F. & Armstrong, P. M. Prevalence and genetic characterization of Powassan virus strains infecting *Ixodes scapularis* in Connecticut. *The American Journal of Tropical Medicine and Hygiene* **87**, 754–759 (2012).
32. Brackney, D. E., Nofchissey, R. A., Fitzpatrick, K. A., Brown, I. K. & Ebel, G. D. Short report: Stable prevalence of Powassan virus in *Ixodes scapularis* in a northern Wisconsin Focus. *The American Journal of Tropical Medicine and Hygiene* **79**, 971–973 (2008).
33. Fish, D. Range expansion of Ixodes scapularis in the USA. in *Climate, Ticks and Disease* (ed. Nuttall, P.) 176–182 (CABI, 2021).
34. Klitting, R. *et al.* Predicting the evolution of the Lassa virus endemic area and population at risk over the next decades. *Nat. Commun.* **13**, 1–15 (2022).
35. Dellicour, S. *et al.* Epidemiological hypothesis testing using a phylogeographic and phylodynamic framework. *Nat. Commun.* **11**, 5620 (2020).
36. Dellicour, S. *et al.* Using phylogeographic approaches to analyse the dispersal history,

velocity and direction of viral lineages - Application to rabies virus spread in Iran. *Mol. Ecol.* **28**, 4335–4350 (2019).
37. Dellicour, S. *et al.* Using viral gene sequences to compare and explain the heterogeneous spatial dynamics of virus epidemics. *Mol. Biol. Evol.* **34**, 2563–2571 (2017).
38. Eisen, R. J. & Eisen, L. The Blacklegged Tick, Ixodes scapularis: An Increasing Public Health Concern. *Trends Parasitol.* **34**, 295–309 (2018).
39. Wang, I. N. *et al.* Genetic diversity of ospC in a local population of Borrelia burgdorferi sensu stricto. *Genetics* **151**, 15–30 (1999).
40. Costero, A. & Grayson, M. A. Experimental transmission of Powassan Virus (Flaviviridae) by *Ixodes scapularis* ticks (Acari: Ixodidae). *The American Journal of Tropical Medicine and Hygiene* **55**, 536–546 (1996).
41. Rogic, A., Tessier, N., Legendre, P., Lapointe, F.-J. & Millien, V. Genetic structure of the white-footed mouse in the context of the emergence of Lyme disease in southern Québec. *Ecol. Evol.* **3**, 2075–2088 (2013).
42. Howell, P. E., Delgado, M. L. & Scribner, K. T. Landscape genetic analysis of co-distributed white-footed mice (Peromyscus leucopus) and prairie deer mice (Peromyscus maniculatus bairdii) in an agroecosystem. *J. Mammal.* **98**, 793–803 (2017).
43. Labuda, M., Danielova, V., Jones, L. D. & Nuttall, P. A. Amplification of tick-borne encephalitis virus infection during co-feeding of ticks. *Med. Vet. Entomol.* **7**, 339–342 (1993).
44. Randolph, S. E., Gern, L. & Nuttall, P. A. Co-feeding ticks: Epidemiological significance for tick-borne pathogen transmission. *Parasitol. Today* **12**, 472–479 (1996).
45. Dupuis, A. P. *et al.* Isolation of deer tick virus (Powassan virus, lineage II) from *Ixodes scapularis* and detection of antibody in vertebrate hosts sampled in the Hudson Valley, New York State. *Parasites & Vectors* **6**, 185 (2013).
46. Aliota, M. T. *et al.* The prevalence of zoonotic tick-borne pathogens in *Ixodes scapularis* collected in the Hudson Valley, New York state. *Vector-borne and Zoonotic Diseases* **14**, 245–250 (2014).
47. Robich, R. M. *et al.* Prevalence and genetic characterization of deer tick virus (Powassan virus, lineage II) in *Ixodes scapularis* ticks collected in Maine. *Am. J. Trop. Med. Hyg.* **101**, 467–471 (2019).
48. Yuan, Q. *et al.* Active surveillance of pathogens from ticks collected in New York State suburban parks and schoolyards. *Zoonoses Public Health* **67**, 684–696 (2020).
49. Matranga, C. B. *et al.* Enhanced methods for unbiased deep sequencing of Lassa and Ebola RNA viruses from clinical and biological samples. *Genome Biol.* **15**, 519 (2014).
50. Grubaugh Lab. Protocols in development. http://grubaughlab.com/open-science/protocols/.
51. Grubaugh, N. D. *et al.* An amplicon-based sequencing framework for accurately measuring intrahost virus diversity using PrimalSeq and iVar. *Genome Biol.* **20**, 8 (2019).
52. Quick, J. *et al.* Multiplex PCR method for MinION and Illumina sequencing of Zika and other virus genomes directly from clinical samples. *Nat. Protoc.* **12**, 1261–1276 (2017).
53. Andersen Lab. Protocols. https://andersen-lab.com/secrets/protocols/ (2017).
54. Nguyen, L.-T., Schmidt, H. A., von Haeseler, A. & Minh, B. Q. IQ-TREE: a fast and effective stochastic algorithm for estimating maximum-likelihood phylogenies. *Mol. Biol. Evol.* **32**, 268–274 (2015).
55. Duchene, S. *et al.* Temporal signal and the phylodynamic threshold of SARS-CoV-2. *Virus Evol* **6**, veaa061 (2020).
56. Baele, G., Lemey, P. & Suchard, M. A. Genealogical Working Distributions for Bayesian Model Testing with Phylogenetic Uncertainty. *Syst. Biol.* **65**, 250–264 (2016).
57. Lemey, P., Rambaut, A., Drummond, A. J. & Suchard, M. A. Bayesian phylogeography finds its

roots. *PLoS Comput. Biol.* **5**, e1000520 (2009).
58. Suchard, M. A. *et al.* Bayesian phylogenetic and phylodynamic data integration using BEAST 1.10. *Virus Evol* **4**, vey016 (2018).
59. Drummond, A. J., Ho, S. Y. W., Phillips, M. J. & Rambaut, A. Relaxed phylogenetics and dating with confidence. *PLoS Biol.* **4**, e88 (2006).
60. Tavaré, S. Some probabilistic and statistical problems in the analysis of DNA sequenced. *Lectures of the Mathematics in the Life Sciences* **17**, 57–86 (1986).
61. Gill, M. S. *et al.* Improving Bayesian population dynamics inference: a coalescent-based model for multiple loci. *Mol. Biol. Evol.* **30**, 713–724 (2013).
62. Rambaut, A., Drummond, A. J., Xie, D., Baele, G. & Suchard, M. A. Posterior Summarization in Bayesian Phylogenetics Using Tracer 1.7. *Syst. Biol.* **67**, 901–904 (2018).
63. Vrancken, B. *et al.* Dynamics and Dispersal of Local Human Immunodeficiency Virus Epidemics Within San Diego and Across the San Diego-Tijuana Border. *Clin. Infect. Dis.* **73**, e2018–e2025 (2021).
64. Trovão, N. S. *et al.* Host ecology determines the dispersal patterns of a plant virus. *Virus Evol* **1**, vev016 (2015).
65. Lemey, P., Rambaut, A., Welch, J. J. & Suchard, M. A. Phylogeography takes a relaxed random walk in continuous space and time. *Mol. Biol. Evol.* **27**, 1877–1885 (2010).
66. Pybus, O. G. *et al.* Unifying the spatial epidemiology and molecular evolution of emerging epidemics. *Proc. Natl. Acad. Sci. U. S. A.* **109**, 15066–15071 (2012).
67. Dellicour, S., Rose, R. & Pybus, O. G. Explaining the geographic spread of emerging epidemics: a framework for comparing viral phylogenies and environmental landscape data. *BMC Bioinformatics* **17**, 82 (2016).
68. Dellicour, S., Rose, R., Faria, N. R., Lemey, P. & Pybus, O. G. SERAPHIM: studying environmental rasters and phylogenetically informed movements. *Bioinformatics* **32**, 3204–3206 (2016).
69. Dellicour, S., Vrancken, B., Trovão, N. S., Fargette, D. & Lemey, P. On the importance of negative controls in viral landscape phylogeography. *Virus Evol* **4**, vey023 (2018).
70. Suchard, M. A., Weiss, R. E. & Sinsheimer, J. S. Models for estimating bayes factors with applications to phylogeny and tests of monophyly. *Biometrics* **61**, 665–673 (2005).
71. Dijkstra, E. W. A note on two problems in connexion with graphs. *Numer. Math.* **1**, 269–271 (1959).
72. McRae, B. H. Isolation by resistance. *Evolution* **60**, 1551–1561 (2006).
73. Jacquot, M., Nomikou, K., Palmarini, M., Mertens, P. & Biek, R. Bluetongue virus spread in Europe is a consequence of climatic, landscape and vertebrate host factors as revealed by phylogeographic inference. *Proc. Biol. Sci.* **284**, (2017).
74. Goodman, L. B. *et al.* High-throughput Detection of Respiratory Pathogens in Animal Specimens by Nanoscale PCR. *J. Vis. Exp.* (2016) doi:10.3791/54781.
75. Klitting, R. *et al.* Predicting the evolution of Lassa Virus endemic area and population at risk over the next decades. *bioRxiv* 2021.09.22.461380 (2021) doi:10.1101/2021.09.22.461380.

Acknowledgements

We would like to thank Anne Piantadosi, Erica Normandin, Pardis C. Sabeti, Rebekah McMinn, Greg Ebel, Heidi Goethert, Sam R. Telford III, Sebastian Lequime, Alexander A. Fisher, and Marc A. Suchard for their input in discussions on the methods and results of this study.

Funding

This publication was made possible by CTSA Grant Number UL1 TR001863 from the National Center for Advancing Translational Science (NCATS), a component of the National Institutes of Health (NIH) awarded to CBFV, and the National Institute Of Allergy And Infectious Diseases of the NIH under Award Number 1R56 AI149004-01A1 awarded to NDG. Its contents are solely the responsibility of the authors and do not necessarily represent the official views of NIH. GB acknowledges support from the Internal Funds KU Leuven under grant agreement C14/18/094 and the Research Foundation - Flanders ("Fonds voor Wetenschappelijk Onderzoek - Vlaanderen," G0E1420N, G098321N).

Author contributions

CBFV, SD, NDG designed the study; DEB, APD, RMR, SCW, JFA, CBL, REL, MAP, LDK, JLG-K, LBG, RPS, PMA, and ATC collected data/samples; CBFV and JRF performed sequencing; CBFV, AFB, GB, SD, NDG analyzed the data; CBFV, SD, and NDG drafted the manuscript; all authors reviewed and approved the manuscript.

Competing interests

NDG is a consultant for Tempus Labs and the National Basketball Association for work related to COVID-19. All other authors declare no competing interests.

Supplementary information

Supplementary Table 1: Nucleic acid extraction and Powassan screening methods used by institutes providing samples.

Institute	Nucleic acid extraction	Powassan virus detection	Reference
CAES	Omega Mag-bind Viral DNA/RNA QIAamp viral RNA mini kit protocol	ENV RT-qPCR	[31]
MHIR	TRIzol Qiagen QIAmp Viral RNA Mini Kit	ENV or NS5 RT-qPCR	[47]
NYSDOH	MagMax Total Nucleic Acid Extraction kit	NS5 RT-qPCR	[45,46]
Cornell	MagMax Total Nucleic Acid Extraction kit	OpenArray Tick Nanochip	[48,74]

Abbreviations: CAES = Connecticut Agricultural Experiment Station, MHIR = MaineHealth Institute for Research, NYSDOH = New York State Department of Health.

Supplementary Table 2: PrimalSeq primer scheme for Powassan virus amplicon-based sequencing.

Primer Name	Sequence	Pool	Start	End
POWV_1_LEFT	ACGTGAGTGTGTTGAGRAAAAGA	1	37	60
POWV_1_RIGHT	AGCCATCAAAGCCATTACCAAGA	1	421	398
POWV_2_LEFT	AGAGTCATTGGAAACTTGATGCAGA	2	322	347
POWV_2_RIGHT	CACAGACCTTCTCCCCCTGAAT	2	706	684
POWV_3_LEFT	TGTTGATGTGGATTGTTTTTGCCG	1	609	633
POWV_3_RIGHT	CCAAGCTCCAGAACCAGGGATA	1	1008	986
POWV_4_LEFT	CCTGTATACGCCACGAGATGCA	2	913	935
POWV_4_RIGHT	CACAGGCCACTATGCTTCCTTT	2	1274	1252
POWV_5_LEFT	YACGCTTCCAGAGGAACACCAG	1	1164	1186
POWV_5_RIGHT	AGGTCTTCGAACCAGTCACGAT	1	1593	1571

POWV_6_LEFT	CAAGTGGAATTGATGTCGCCCA	2	1490	1512
POWV_6_RIGHT	ACTGTGTCATGACCACTGTCCA	2	1902	1880
POWV_7_LEFT	ACCTGTGATGTGGGACTTGAAAA	1	1789	1812
POWV_7_RIGHT	CCCACTGAACCAAAGTCCCATG	1	2208	2186
POWV_8_LEFT	TGGTTCCAGAAAGGCAGTACCA	2	2101	2123
POWV_8_RIGHT	TCCACACAACTAGGCCTTCTCC	2	2483	2461
POWV_9_LEFT	ACCCTGATGATGACAATGGGAGT	1	2386	2409
POWV_9_RIGHT	CTTGCCCCAACTCTTCCATGAC	1	2782	2760
POWV_10_LEFT	TGGTAGACAAGACAGATCCAGCA	2	2681	2704
POWV_10_RIGHT	GCTGGCCATGTACAGTTTCGAA	2	3102	3080
POWV_11_LEFT	CATTCACACGGAYCAGAGCATG	1	2997	3019
POWV_11_RIGHT	ATACCAACAATCTGTGCCGCTG	1	3415	3393
POWV_12_LEFT	AGCCTCAGTTAGAAGCACCACA	2	3306	3328
POWV_12_RIGHT	GCATGCTAAAAACTGCCTGCAG	2	3737	3715
POWV_13_LEFT	TTAGAGTGGAGGAGATCGTGCG	1	3626	3648
POWV_13_RIGHT	TCCATGGTGAACAGCAGTCAGA	1	3991	3969
POWV_14_LEFT	GCCATGGGACTACTCATAATYAAGGC	2	3880	3906
POWV_14_RIGHT	ATGAGAAAGGAACCAGCCGAGA	2	4278	4256
POWV_15_LEFT	AACTGTGGTGGGGGTCATGTTA	1	4182	4204
POWV_15_RIGHT	CTCCCCATGGTCAGACAATTGC	1	4600	4578
POWV_16_LEFT	CTGGTGACAATGGGGGCATGGA	2	4504	4526
POWV_16_RIGHT	TCAGTTTCCCTGGTTGGCATTG	2	4913	4891
POWV_17_LEFT	GCTTGGAAGGAAAATGGGGAGG	1	4817	4839
POWV_17_RIGHT	GCTCGGGAAGGACTCTATGTGT	1	5195	5173
POWV_18_LEFT	CGTTGAGAAAAGCCGACCAGAA	2	5070	5092
POWV_18_RIGHT	ACGCGCATCTGTTCTCTTTAGC	2	5510	5488
POWV_19_LEFT	TTGGGAGGTGGCCATAATGGAT	1	5409	5431
POWV_19_RIGHT	TCTGAGATGTCGGTCGTCACAA	1	5814	5792
POWV_20_LEFT	TGAGGCAGAAAGGGAAAAGTGTG	2	5702	5725
POWV_20_RIGHT	CATTTTCCCTTGTTCTGGCCCA	2	6115	6093
POWV_21_LEFT	CTCTGGTGCAGTGGAAAGAAGC	1	6017	6039
POWV_21_RIGHT	ATCCCTTCCTTCCCGGAACATT	1	6388	6366
POWV_22_LEFT	ATGGTCCTGATGGTGAACTGGT	2	6284	6306
POWV_22_RIGHT	CAGAACCATCCTGCTAACCGAC	2	6670	6648
POWV_23_LEFT	CATGTTGACGCTTCTGGAGGTG	1	6573	6595
POWV_23_RIGHT	GGCGGGCTGTATGTCAATGTTT	1	6985	6963
POWV_24_LEFT	TTGGAGAGAACAAAAGCCGACA	2	6886	6908
POWV_24_RIGHT	TCTAGCCCAGATGTGACCACAG	2	7257	7235
POWV_25_LEFT	CATTTTTCGGTGTGGCTGGACAC	1	7127	7150
POWV_25_RIGHT	CTTTCCTCCTCTGGCCTCAACA	1	7515	7493
POWV_26_LEFT	GAAAGATGAGCYTGCTCCTTGC	2	7379	7401
POWV_26_RIGHT	TCTCGGTTGGTCTCCATGACTC	2	7740	7718
POWV_27_LEFT	TCAGAACTCAGGGGGCTAGAAG	1	7604	7626
POWV_27_RIGHT	CATCCAAGGCTCGTCACCAATC	1	7989	7967
POWV_28_LEFT	CACTCAAGGGAGAAGTCGTGGA	2	7841	7863
POWV_28_RIGHT	TCCACCCCACTGTAGCTGAAAA	2	8242	8220
POWV_29_LEFT	TGGAAAGCCAGGAATCCAGACG	1	8137	8159
POWV_29_RIGHT	GGGTGTTCCTTGTCTTCATGCC	1	8526	8504
POWV_30_LEFT	GACACTGGCAGAAGACAAGGTG	2	8424	8446
POWV_30_RIGHT	GGCTGTGAAGGTGCTCAAGTAG	2	8792	8770
POWV_31_LEFT	GCAACAGCGCGTTTTCAAAGAA	1	8679	8701
POWV_31_RIGHT	TCAAACTCAAGGAAACGGCTCC	1	9090	9068
POWV_32_LEFT	GGGAAAGAGAGAGAAGAAGCTGG	2	8994	9017
POWV_32_RIGHT	GCCTGGCAACCTTAACCACTTT	2	9377	9355
POWV_33_LEFT	AGCAGATCCTTCGGTACATGGA	1	9281	9303
POWV_33_RIGHT	AGTACAGGGCCTTTCCAAACCT	1	9668	9646

POWV_34_LEFT	AGGATCCCCGTCTGAAAAGGGT	2	9536	9558
POWV_34_RIGHT	CATCTGCCCATACGCTTTGGAC	2	9913	9891
POWV_35_LEFT	CTGCAGAGATCAAGACGAGCTG	1	9810	9832
POWV_35_RIGHT	CCCAGATGTTCTTGGCCCATTC	1	10223	10201
POWV_36_LEFT	ACAAATGGTGGATGAATGGAGAGAT	2	10110	10135
POWV_36_RIGHT	TTTAGCAGCCATGAGGGTCTCA	2	10478	10456
POWV_37_LEFT	GAGACTATTTGGCAAACATGGACAGA	1	10268	10294
POWV_37_RIGHT	GGGGCTCTAGAATGGCCTAACT	1	10638	10616

Supplementary Table 3: Newly sequenced Powassan virus genomes.

Source	Sample	Accession
CAES	PV001-P1734_LII_Bridgeport_CT_USA_Ixodes-scapularis_F_Drag_2014-10-29	OL704116
CAES	PV002-P1735_LII_Bridgeport_CT_USA_Ixodes-scapularis_M_Drag_2014-10-29	OL704117
CAES	PV003-P1663_LII_North-Branford_CT_USA_Ixodes-scapularis_F_Drag_2014-10-30	OL704118
CAES	PV004-P1665_LII_North-Branford_CT_USA_Ixodes-scapularis_F_Drag_2014-10-30	OL704119
CAES	PV005-P1666_LII_North-Branford_CT_USA_Ixodes-scapularis_M_Drag_2014-10-30	OL704120
CAES	PV006-P1677_LII_North-Branford_CT_USA_Ixodes-scapularis_F_Drag_2014-10-30	OL704121
CAES	PV007-P1384_LII_Bridgeport_CT_USA_Ixodes-scapularis_F_Drag_2014-05-02	OL704122
CAES	PV008-P1429_LII_North-Branford_CT_USA_Ixodes-scapularis_N_Drag_2014-06-24	OL704123
CAES	PV009-P1742_LII_North-Branford_CT_USA_Ixodes-scapularis_F_Drag_2014-10-27	OL704124
CAES	PV010-P1783A_LII_North-Branford_CT_USA_Ixodes-scapularis_F_Drag_2014-10-30	OL704125
CAES	PV011-P1774A_LII_North-Branford_CT_USA_Ixodes-scapularis_F_Drag_2014-10-28	OL704126
CAES	PV012-P913_LII_Bridgeport_CT_USA_Ixodes-scapularis_N_Drag_2013-06-12	OL704127
CAES	PV013-P2552_LII_Bridgeport_CT_USA_Ixodes-scapularis_M_Drag_2015-10-22	OL704128
CAES	PV014-8_LII_Redding_CT_USA_Ixodes-scapularis_F_Drag_2015-12-28	OL704129
CAES	PV015-67_LII_North-Branford_CT_USA_Ixodes-scapularis_F_Drag_2015-12-03	OL704130
CAES	PV016-32_LII_Redding_CT_USA_Ixodes-scapularis_F_Drag_2016-11-10	OL704131
CAES	PV017-45_LII_Lyme_CT_USA_Ixodes-scapularis_F_Drag_2016-11-28	OL704132
CAES	PV018-50_LII_Lyme_CT_USA_Ixodes-scapularis_M_Drag_2016-11-28	OL704133
CAES	PV019-52_LII_Lyme_CT_USA_Ixodes-scapularis_M_Drag_2016-11-28	OL704134
CAES	PV020-53_LII_Lyme_CT_USA_Ixodes-scapularis_M_Drag_2016-11-28	OL704135
CAES	PV021-55_LII_Lyme_CT_USA_Ixodes-scapularis_F_Drag_2016-11-28	OL704136
CAES	PV022-62_LII_Lyme_CT_USA_Ixodes-scapularis_M_Drag_2016-11-16	OL704137
CAES	PV023-93_LII_Lyme_CT_USA_Ixodes-scapularis_F_Drag_2016-11-07	OL704138
CAES	PV024-95_LII_Lyme_CT_USA_Ixodes-scapularis_F_Drag_2016-11-07	OL704139
CAES	PV025-98_LII_Lyme_CT_USA_Ixodes-scapularis_F_Drag_2016-11-07	OL704140
CAES	PV026-101_LII_Lyme_CT_USA_Ixodes-scapularis_F_Drag_2016-11-07	OL704141
CAES	PV027-114_LII_Lyme_CT_USA_Ixodes-scapularis_M_Drag_2016-11-01	OL704142
CAES	PV028-116_LII_Lyme_CT_USA_Ixodes-scapularis_M_Drag_2016-11-01	OL704143
CAES	PV029-118_LII_Lyme_CT_USA_Ixodes-scapularis_M_Drag_2016-11-01	OL704144
CAES	PV030-122_LII_Lyme_CT_USA_Ixodes-scapularis_F_Drag_2016-11-01	OL704145
CAES	PV031-124_LII_Lyme_CT_USA_Ixodes-scapularis_F_Drag_2016-11-01	OL704146
CAES	PV032-125_LII_Lyme_CT_USA_Ixodes-scapularis_F_Drag_2016-11-01	OL704147
CAES	PV033-126_LII_Lyme_CT_USA_Ixodes-scapularis_F_Drag_2016-11-01	OL704148
CAES	PV034-P0375_LII_Bridgeport_CT_USA_Ixodes-scapularis_M_Drag_2010-11-01	OL704149
CAES	PV035-P0183_LII_Bridgeport_CT_USA_Ixodes-scapularis_F_Drag_2008-11-01	OL704150
CAES	PV036-P0096_LII_Bridgeport_CT_USA_Ixodes-scapularis_F_Drag_2008-11-01	OL704151
CAES	PV037-P0494_LII_Bridgeport_CT_USA_Ixodes-scapularis_F_Drag_2010-11-02	OL704152
CAES	PV038-P0525_LII_North-Branford_CT_USA_Ixodes-scapularis_F_Drag_2010-10-29	OL704153
CAES	PV039-P0526_LII_North-Branford_CT_USA_Ixodes-scapularis_F_Drag_2010-10-29	OL704154
CAES	PV040-P0618_LII_North-Branford_CT_USA_Ixodes-scapularis_F_Drag_2010-10-29	OL704155
CAES	PV041-P0621_LII_North-Branford_CT_USA_Ixodes-scapularis_F_Drag_2010-10-29	OL704156
CAES	PV042-P0629_LII_North-Branford_CT_USA_Ixodes-scapularis_M_Drag_2010-10-29	OL704157
CAES	PV043-P1697_LII_Bridgeport_CT_USA_Ixodes-scapularis_F_Drag_2011-11-09	OL704158
CAES	PV045-P0690_LII_North-Branford_CT_USA_Ixodes-scapularis_M_Drag_2011-04-26	OL704159
CAES	PV046-P0681_LII_North-Branford_CT_USA_Ixodes-scapularis_M_Drag_2011-04-26	OL704160

CAES	PV047-P0785_LII_North-Branford_CT_USA_Ixodes-scapularis_M_Drag_2011-05-09	OL704161
CAES	PV048-P0751_LII_Bridgeport_CT_USA_Ixodes-scapularis_F_Drag_2011-04-27	OL704162
CAES	PV049-P0760_LII_Bridgeport_CT_USA_Ixodes-scapularis_M_Drag_2011-04-27	OL704163
CAES	PV050-P0795_LII_North-Branford_CT_USA_Ixodes-scapularis_F_Drag_2011-05-09	OL704164
CAES	PV051-P0933_LII_North-Branford_CT_USA_Ixodes-scapularis_F_Drag_2011-10-21	OL704165
CAES	PV052-P1113_LII_Bridgeport_CT_USA_Ixodes-scapularis_M_Drag_2011-10-18	OL704166
CAES	PV053-P1104_LII_Bridgeport_CT_USA_Ixodes-scapularis_M_Drag_2011-10-18	OL704167
CAES	PV054-P1109_LII_Bridgeport_CT_USA_Ixodes-scapularis_F_Drag_2011-10-18	OL704168
CAES	PV055-P1112_LII_Bridgeport_CT_USA_Ixodes-scapularis_F_Drag_2011-10-18	OL704169
CAES	PV056-P1114_LII_Bridgeport_CT_USA_Ixodes-scapularis_M_Drag_2011-10-18	OL704170
CAES	PV057-P1107_LII_Bridgeport_CT_USA_Ixodes-scapularis_F_Drag_2011-10-18	OL704171
CAES	PV058-P1241_LII_Bridgeport_CT_USA_Ixodes-scapularis_F_Drag_2011-10-28	OL704172
CAES	PV059-P1514_LII_Bridgeport_CT_USA_Ixodes-scapularis_M_Drag_2011-10-25	OL704173
CAES	PV060-P1518_LII_Bridgeport_CT_USA_Ixodes-scapularis_F_Drag_2011-10-25	OL704174
CAES	PV061-P1730_LII_Bridgeport_CT_USA_Ixodes-scapularis_F_Drag_2011-11-09	OL704175
CAES	PV062-P1753_LII_Bridgeport_CT_USA_Ixodes-scapularis_M_Drag_2011-11-09	OL704176
CAES	PV063-P1912_LII_Bridgeport_CT_USA_Ixodes-scapularis_M_Drag_2012-04-05	OL704177
CAES	PV064-P1933_LII_Bridgeport_CT_USA_Ixodes-scapularis_F_Drag_2012-04-05	OL704178
CAES	PV065-P1930_LII_Bridgeport_CT_USA_Ixodes-scapularis_F_Drag_2012-04-05	OL704179
CAES	PV066-P1184_LII_North-Branford_CT_USA_Ixodes-scapularis_N_Drag_2014-05-29	OL704180
CAES	PV067-P1290_LII_North-Branford_CT_USA_Ixodes-scapularis_Mix_Drag_2014-05-29	OL704181
CAES	PV068-P1295_LII_North-Branford_CT_USA_Ixodes-scapularis_Mix_Drag_2014-05-14	OL704182
CAES	PV069-165_LII_Redding_CT_USA_Ixodes-scapularis_M_Drag_2016-11-10	OL704183
CAES	PV070-188_LII_North-Branford_CT_USA_Ixodes-scapularis_F_Drag_2016-12-06	OL704184
CAES	PV071-219_LII_Redding_CT_USA_Ixodes-scapularis_M_Drag_2016-11-14	OL704185
CAES	PV072-228_LII_Redding_CT_USA_Ixodes-scapularis_M_Drag_2016-11-14	OL704186
CAES	PV073-237_LII_Redding_CT_USA_Ixodes-scapularis_F_Drag_2016-11-14	OL704187
CAES	PV074-3338_LII_Groton_CT_USA_Ixodes-scapularis_F_Drag_2016-11-02	OL704188
CAES	PV075-3381_LII_Groton_CT_USA_Ixodes-scapularis_F_Drag_2016-11-02	OL704189
CAES	PV076-3464_LII_Groton_CT_USA_Ixodes-scapularis_F_Drag_2016-11-02	OL704190
CAES	PV077-3569_LII_North-Branford_CT_USA_Ixodes-scapularis_F_Drag_2016-10-17	OL704191
CAES	PV078-3591_LII_North-Branford_CT_USA_Ixodes-scapularis_M_Drag_2016-10-20	OL704192
CAES	PV080-160_LII_North-Branford_CT_USA_Ixodes-scapularis_Unknown_Drag_2016-12-01	OL704193
CAES	PV111-69_LII_Westport_CT_USA_Ixodes-scapularis_F_Drag_2019-04-09	OL704194
CAES	PV112-140_LII_Lyme_CT_USA_Ixodes-scapularis_F_Drag_2019-04-17	OL704195
CAES	PV113-364_LII_Westport_CT_USA_Ixodes-scapularis_F_Drag_2019-05-07	OL704196
CAES	PV114-375_LII_North-Branford_CT_USA_Ixodes-scapularis_F_Drag_2019-05-08	OL704197
Cornell	PV299-LI108_LII_Mill-Neck_NY_USA_Ixodes-scapularis_F_Drag_2018-10-25	OL704210
Cornell	PV300-LI131_LII_Mill-Neck_NY_USA_Ixodes-scapularis_M_Drag_2018-10-25	OL704209
Cornell	PV301-LI132_LII_Mill-Neck_NY_USA_Ixodes-scapularis_M_Drag_2018-10-25	OL704208
Cornell	PV302-LI171_LII_Mill-Neck_NY_USA_Ixodes-scapularis_F_Drag_2018-10-25	OL704207
Cornell	PV303-LI192_LII_Mill-Neck_NY_USA_Ixodes-scapularis_M_Drag_2018-10-25	OL704206
Cornell	PV305-LI212_LII_Mill-Neck_NY_USA_Ixodes-scapularis_M_Drag_2018-10-25	OL704205
Cornell	PV306-LI298_LII_Oyster-Bay_NY_USA_Ixodes-scapularis_F_Drag_2018-10-31	OL704204
Cornell	PV307-LI305_LII_Oyster-Bay_NY_USA_Ixodes-scapularis_F_Drag_2018-10-31	OL704203
Cornell	PV309-LI327_LII_Oyster-Bay_NY_USA_Ixodes-scapularis_M_Drag_2018-10-31	OL704202
Cornell	PV310-LI331_LII_Oyster-Bay_NY_USA_Ixodes-scapularis_M_Drag_2018-10-31	OL704201
Cornell	PV311-LI336_LII_Oyster-Bay_NY_USA_Ixodes-scapularis_M_Drag_2018-10-31	OL704200
Cornell	PV312-LI343_LII_Oyster-Bay_NY_USA_Ixodes-scapularis_M_Drag_2018-10-31	OL704199
Cornell	PV313-LI586_LII_Woodbury_NY_USA_Ixodes-scapularis_M_Drag_2018-12-04	OL704198
MHIR	PV083-242_LII_Cape-Elizabeth_ME_USA_Ixodes-scapularis_N_Drag_2016-06-13	OL704212
MHIR	PV084-612_LII_Wells_ME_USA_Ixodes-scapularis_F_Drag_2016-10-07	OL704213
MHIR	PV085-632_LII_Wells_ME_USA_Ixodes-scapularis_F_Drag_2016-10-07	OL704214
MHIR	PV086-687_LII_Midcoast_ME_USA_Ixodes-scapularis_F_Drag_2016-10-14	OL704215
MHIR	PV087-946_LII_Cape-Elizabeth_ME_USA_Ixodes-scapularis_M_Drag_2016-10-06	OL704216
MHIR	PV088-963_LII_Wells_ME_USA_Ixodes-scapularis_M_Drag_2016-11-07	OL704217

MHIR	PV089-1003_LII_Wells_ME_USA_Ixodes-scapularis_F_Drag_2016-11-07	OL704218
MHIR	PV090-1135_LII_Wells_ME_USA_Ixodes-scapularis_M_Drag_2016-11-09	OL704219
MHIR	PV091-1141_LII_Wells_ME_USA_Ixodes-scapularis_M_Drag_2016-11-09	OL704220
MHIR	PV093-1331_LII_Standish_ME_USA_Ixodes-scapularis_M_Drag_2016-11-17	OL704222
MHIR	PV094-1341_LII_Standish_ME_USA_Ixodes-scapularis_M_Drag_2016-11-17	OL704223
MHIR	PV096-CO18_LII_Cape-Elizabeth_ME_USA_Ixodes-scapularis_M_Drag_2017-11-15	OL704224
MHIR	PV098-CO57_LII_Cape-Elizabeth_ME_USA_Ixodes-scapularis_F_Drag_2017-11-15	OL704226
MHIR	PV102-CO166_LII_Cape-Elizabeth_ME_USA_Ixodes-scapularis_F_Drag_2017-11-15	OL704230
MHIR	PV103-CO527_LII_Cape-Elizabeth_ME_USA_Ixodes-scapularis_M_Drag_2017-11-15	OL704231
MHIR	PV105-CO570_LII_Cape-Elizabeth_ME_USA_Ixodes-scapularis_M_Drag_2017-11-07	OL704233
MHIR	PV106-CO574_LII_Cape-Elizabeth_ME_USA_Ixodes-scapularis_M_Drag_2017-11-07	OL704234
MHIR	PV109-CO452_LII_Wells_ME_USA_Ixodes-scapularis_F_Drag_2017-11-15	OL704236
MHIR	PV286-POW19-088_LII_Thomaston_ME_USA_Ixodes-scapularis_M_Drag_2019-05-22	OL704237
MHIR	PV287-WB19-061_LII_Wells_ME_USA_Ixodes-scapularis_N_Bird_2019-06-18	OL704238
MHIR	PV292-PF3.019_LII_Wells_ME_USA_Ixodes-scapularis_M_Drag_2018-06-07	OL704239
MHIR	PV293-PF3.020_LII_Wells_ME_USA_Ixodes-scapularis_M_Drag_2018-06-07	OL704240
MHIR	PV297-PF1.021_LII_Wells_ME_USA_Ixodes-scapularis_M_Drag_2018-06-19	OL704241
MHIR	PV298-PF6.005_LII_Wells_ME_USA_Ixodes-scapularis_M_Drag_2018-06-14	OL704242
MHIR	PV081.2-H11_LII_Cape-Elizabeth_ME_USA_Ixodes-scapularis_M_Drag_2016-04-08	OL704211
MHIR	PV092.2-1217_LII_Cape-Elizabeth_ME_USA_Ixodes-scapularis_F_Drag_2016-11-18	OL704221
MHIR	PV097.2-CO46_LII_Cape-Elizabeth_ME_USA_Ixodes-scapularis_F_Drag_2017-11-15	OL704225
MHIR	PV099.2-CO68_LII_Cape-Elizabeth_ME_USA_Ixodes-scapularis_F_Drag_2017-11-15	OL704227
MHIR	PV100.2-CO95_LII_Cape-Elizabeth_ME_USA_Ixodes-scapularis_M_Drag_2017-11-15	OL704228
MHIR	PV101.2-CO110_LII_Cape-Elizabeth_ME_USA_Ixodes-scapularis_F_Drag_2017-11-15	OL704229
MHIR	PV104.2-CO542_LII_Cape-Elizabeth_ME_USA_Ixodes-scapularis_F_Drag_2017-11-15	OL704232
MHIR	PV108.2-CO239_LII_Wells_ME_USA_Ixodes-scapularis_M_Drag_2017-11-15	OL704235
NYSDOH	PV116-18079-121_LII_Brewster_NY_USA_Ixodes-scapularis_M_Drag_2018-10-24	OL704243
NYSDOH	PV117-18087-108_LII_Montebello_NY_USA_Ixodes-scapularis_F_Drag_2018-10-26	OL704244
NYSDOH	PV118-18087-113_LII_Montebello_NY_USA_Ixodes-scapularis_M_Drag_2018-10-26	OL704245
NYSDOH	PV119-18119-217_LII_Mohansic_NY_USA_Ixodes-scapularis_M_Drag_2018-10-22	OL704246
NYSDOH	PV120-18119-218_LII_Mohansic_NY_USA_Ixodes-scapularis_M_Drag_2018-10-22	OL704247
NYSDOH	PV121-18119-219_LII_Mohansic_NY_USA_Ixodes-scapularis_M_Drag_2018-10-22	OL704248
NYSDOH	PV122-18119-228_LII_Armonk_NY_USA_Ixodes-scapularis_M_Drag_2018-10-31	OL704249
NYSDOH	PV123-17091-200_LII_Saratoga-Springs_NY_USA_Ixodes-scapularis_N_Drag_2017-07-20	OL704250
NYSDOH	PV124-17119-057_LII_Armonk_NY_USA_Ixodes-scapularis_N_Drag_2017-06-13	OL704251
NYSDOH	PV125-17119-059_LII_Armonk_NY_USA_Ixodes-scapularis_N_Drag_2017-06-13	OL704252
NYSDOH	PV127-17091-230_LII_Stillwater_NY_USA_Ixodes-scapularis_N_Drag_2017-07-21	OL704253
NYSDOH	PV128-17091-144_LII_Malta_NY_USA_Ixodes-scapularis_F_Drag_2017-07-05	OL704254
NYSDOH	PV129-18095-057_LII_Blenheim_NY_USA_Ixodes-scapularis_F_Drag_2018-06-15	OL704255
NYSDOH	PV130-18021-061_LII_Clermont_NY_USA_Ixodes-scapularis_F_Drag_2018-05-24	OL704256
NYSDOH	PV131-18021-063_LII_Clermont_NY_USA_Ixodes-scapularis_F_Drag_2018-05-24	OL704257
NYSDOH	PV132-17119-2-009_LII_Redding_CT_USA_Ixodes-scapularis_M_Deer_2017-10-28	OL704258
NYSDOH	PV133-17021-480_LII_Clermont_NY_USA_Ixodes-scapularis_F_Drag_2017-11-01	OL704259
NYSDOH	PV134-17091-236_LII_Greenfield_NY_USA_Ixodes-scapularis_N_Drag_2017-07-20	OL704260
NYSDOH	PV135-17021-482_LII_Clermont_NY_USA_Ixodes-scapularis_F_Drag_2017-11-01	OL704261
NYSDOH	PV136-18039-055_LII_Cairo_NY_USA_Ixodes-scapularis_L_Drag_2018-05-31	OL704262
NYSDOH	PV137-16021-172_LII_Greenport_NY_USA_Ixodes-scapularis_M_Drag_2016-10-21	OL704263
NYSDOH	PV138-15-S22-01_LII_Shelter-Island_NY_USA_Ixodes-scapularis_F_Deer_2016-01-07	OL704264
NYSDOH	PV139-15071-117_LII_Wallkill_NY_USA_Ixodes-scapularis_M_Drag_2015-10-21	OL704265
NYSDOH	PV141-17091-11-006_LII_Stillwater_NY_USA_Ixodes-scapularis_M_Deer_2017-11-18	OL704266
NYSDOH	PV142-17091-23-001_LII_Saratoga_NY_USA_Ixodes-scapularis_M_Deer_2017-11-18	OL704267
NYSDOH	PV143-17119-131_LII_Armonk_NY_USA_Ixodes-scapularis_M_Drag_2017-10-25	OL704268
NYSDOH	PV144-17091-27-001_LII_Clifton-Park_NY_USA_Ixodes-scapularis_M_Deer_2017-11-19	OL704269
NYSDOH	PV145-17091-11-002_LII_Stillwater_NY_USA_Ixodes-scapularis_M_Deer_2017-11-18	OL704270
NYSDOH	PV146-17027-241_LII_Holmes_NY_USA_Ixodes-scapularis_M_Drag_2017-10-23	OL704271
NYSDOH	PV147-17119-27-001_LII_Somers_NY_USA_Ixodes-scapularis_M_Deer_2017-11-08	OL704272

NYSDOH	PV148-17079-117_LII_Brewster_NY_USA_Ixodes-scapularis_M_Drag_2017-10-16	OL704273
NYSDOH	PV149-17103-304_LII_Islip_NY_USA_Ixodes-scapularis_M_Drag_2017-05-08	OL704274
NYSDOH	PV150-17103-254_LII_Huntington_NY_USA_Ixodes-scapularis_F_Drag_2017-05-12	OL704275
NYSDOH	PV151-17119-18-001_LII_Pound-Ridge_NY_USA_Ixodes-scapularis_M_Deer_2017-10-28	OL704276
NYSDOH	PV152-12021-250_LII_Clermont_NY_USA_Ixodes-scapularis_M_Drag_2012-11-16	OL704277
NYSDOH	PV153-14CD06-001_LII_Ancram_NY_USA_Ixodes-scapularis_M_Deer_2014-11-15	OL704278
NYSDOH	PV154-14CD13-002_LII_Copake_NY_USA_Ixodes-scapularis_M_Deer_2014-11-15	OL704279
NYSDOH	PV155-14CD34-002_LII_North-Hoosick_NY_USA_Ixodes-scapularis_M_Deer_2014-11-16	OL704280
NYSDOH	PV156-14071-112_LII_Wallkill_NY_USA_Ixodes-scapularis_M_Drag_2014-10-28	OL704281
NYSDOH	PV157-14071-113_LII_Wallkill_NY_USA_Ixodes-scapularis_M_Drag_2014-10-28	OL704282
NYSDOH	PV158-14071-118_LII_Wallkill_NY_USA_Ixodes-scapularis_F_Drag_2014-10-28	OL704283
NYSDOH	PV159-14071-119_LII_Wallkill_NY_USA_Ixodes-scapularis_F_Drag_2014-10-28	OL704284
NYSDOH	PV160-14103-145_LII_Islip_NY_USA_Ixodes-scapularis_M_Drag_2014-11-10	OL704285
NYSDOH	PV161-15CD01-001_LII_East-Taghkanic_NY_USA_Ixodes-scapularis_M_Deer_2015-11-21	OL704286
NYSDOH	PV162-15CD15-001_LII_Ancramdale_NY_USA_Ixodes-scapularis_M_Deer_2015-11-21	OL704287
NYSDOH	PV163-15CD31-001_LII_Copake_NY_USA_Ixodes-scapularis_M_Deer_2015-11-22	OL704288
NYSDOH	PV164-15CD59-002_LII_Poestenkill_NY_USA_Ixodes-scapularis_M_Deer_2015-11-22	OL704289
NYSDOH	PV165-12021-240_LII_Clermont_NY_USA_Ixodes-scapularis_F_Drag_2012-11-16	OL704290
NYSDOH	PV166-18103-2025_LII_Huntington_NY_USA_Ixodes-scapularis_F_Drag_2018-11-19	OL704291
NYSDOH	PV167-18103-1656_LII_East-Hampton_NY_USA_Ixodes-scapularis_F_Drag_2018-10-23	OL704292
NYSDOH	PV168-18103-1536_LII_Islip_NY_USA_Ixodes-scapularis_F_Drag_2018-10-19	OL704293
NYSDOH	PV169-19001-410_LII_Guilderland_NY_USA_Ixodes-scapularis_F_Drag_2019-04-17	OL704294
NYSDOH	PV170-19001-415_LII_Guilderland_NY_USA_Ixodes-scapularis_F_Drag_2019-04-17	OL704295
NYSDOH	PV171-19001-427_LII_Guilderland_NY_USA_Ixodes-scapularis_F_Drag_2019-04-17	OL704296
NYSDOH	PV172-19001-589_LII_Guilderland_NY_USA_Ixodes-scapularis_F_Drag_2019-05-22	OL704297
NYSDOH	PV173-19001-591_LII_Guilderland_NY_USA_Ixodes-scapularis_F_Drag_2019-05-22	OL704298
NYSDOH	PV174-19001-601_LII_Guilderland_NY_USA_Ixodes-scapularis_M_Drag_2019-05-22	OL704299
NYSDOH	PV175-19021-063_LII_Chatham_NY_USA_Ixodes-scapularis_F_Drag_2019-05-07	OL704300
NYSDOH	PV176-19039-010_LII_Greenville_NY_USA_Ixodes-scapularis_M_Drag_2019-05-08	OL704301
NYSDOH	PV177-19091-035_LII_Wilton_NY_USA_Ixodes-scapularis_F_Drag_2019-04-22	OL704302
NYSDOH	PV178-19091-043_LII_Wilton_NY_USA_Ixodes-scapularis_M_Drag_2019-04-22	OL704303
NYSDOH	PV179-19091-084_LII_Saratoga-Springs_NY_USA_Ixodes-scapularis_F_Drag_2019-04-29	OL704304
NYSDOH	PV180-19091-164_LII_Wilton_NY_USA_Ixodes-scapularis_F_Drag_2019-05-15	OL704305
NYSDOH	PV181-19091-165_LII_Wilton_NY_USA_Ixodes-scapularis_F_Drag_2019-05-15	OL704306
NYSDOH	PV182-19093-125_LII_Glenville_NY_USA_Ixodes-scapularis_F_Drag_2019-05-16	OL704307
NYSDOH	PV183-19093-142_LII_Glenville_NY_USA_Ixodes-scapularis_M_Drag_2019-05-16	OL704308
NYSDOH	PV185-19093-242_LII_Glenville_NY_USA_Ixodes-scapularis_M_Drag_2019-05-22	OL704309
NYSDOH	PV186-19115-021_LII_Jackson_NY_USA_Ixodes-scapularis_F_Drag_2019-05-06	OL704310
NYSDOH	PV187-16CD17_LII_Copake_NY_USA_Ixodes-scapularis_M_Deer_2016-11-19	OL704311
NYSDOH	PV188-16021-171_LII_Greenport_NY_USA_Ixodes-scapularis_F_Drag_2016-10-21	OL704312
NYSDOH	PV189-18091-387_LII_Charlton_NY_USA_Ixodes-scapularis_M_Drag_2018-11-08	OL704313
NYSDOH	PV190-18091-16-005_LII_Stillwater_NY_USA_Ixodes-scapularis_M_Deer_2018-11-17	OL704314
NYSDOH	PV191-18091-26-001_LII_Schaghticoke_NY_USA_Ixodes-scapularis_M_Deer_2018-11-18	OL704315
NYSDOH	PV192-18091-11-003_LII_Saratoga_NY_USA_Ixodes-scapularis_M_Deer_2018-11-17	OL704316
NYSDOH	PV193-18091-328_LII_Milton_NY_USA_Ixodes-scapularis_M_Drag_2018-11-07	OL704317
NYSDOH	PV194-18089-048_LII_Hermon_NY_USA_Ixodes-scapularis_F_Drag_2018-10-14	OL704318
NYSDOH	PV195-18089-049_LII_Hermon_NY_USA_Ixodes-scapularis_F_Drag_2018-10-14	OL704319
NYSDOH	PV196-15-S13-03_LII_Shelter-Island_NY_USA_Ixodes-scapularis_M_Deer_2016-01-13	OL704320
NYSDOH	PV197-15-S26-01_LII_Shelter-Island_NY_USA_Ixodes-scapularis_M_Deer_2016-01-20	OL704321
NYSDOH	PV200-15CD63-001_LII_Nassau_NY_USA_Ixodes-scapularis_M_Deer_2015-11-22	OL704322
NYSDOH	PV201-16021-231_LII_Clermont_NY_USA_Ixodes-scapularis_M_Drag_2016-10-25	OL704323
NYSDOH	PV202-17091-180_LII_Saratoga-Springs_NY_USA_Ixodes-scapularis_N_Drag_2017-07-20	OL704324
NYSDOH	PV203-17021-227_LII_Greenport_NY_USA_Ixodes-scapularis_N_Drag_2017-05-24	OL704325
NYSDOH	PV204-19103-1357_LII_Southampton_NY_USA_Ixodes-scapularis_N_Drag_2019-06-17	OL704326
NYSDOH	PV205-19119-078_LII_Armonk_NY_USA_Ixodes-scapularis_N_Drag_2019-05-31	OL704327
NYSDOH	PV206-19103-01-001_LII_Shelter-Island_NY_USA_Ixodes-scapularis_M_Deer_2019-01-07	OL704328

NYSDOH	PV207-19103-14-001_LII_Shelter-Island_NY_USA_Ixodes-scapularis_M_Deer_2019-01-07	OL704329
NYSDOH	PV208-19103-27-001_LII_Shelter-Island_NY_USA_Ixodes-scapularis_M_Deer_2019-01-08	OL704330
NYSDOH	PV209-19103-36-003_LII_Shelter-Island_NY_USA_Ixodes-scapularis_F_Deer_2019-01-08	OL704331
NYSDOH	PV210-19103-37-002_LII_Shelter-Island_NY_USA_Ixodes-scapularis_M_Deer_2019-01-08	OL704332
NYSDOH	PV211-19103-37-004_LII_Shelter-Island_NY_USA_Ixodes-scapularis_F_Deer_2019-01-08	OL704333
NYSDOH	PV212-19103-41-001_LII_Shelter-Island_NY_USA_Ixodes-scapularis_M_Deer_2019-01-08	OL704334
NYSDOH	PV213-19103-43-001_LII_Shelter-Island_NY_USA_Ixodes-scapularis_F_Deer_2019-01-09	OL704335
NYSDOH	PV215-19091-227_LII_Clifton-Park_NY_USA_Ixodes-scapularis_F_Drag_2019-05-31	OL704336
NYSDOH	PV216-19091-231_LII_Clifton-Park_NY_USA_Ixodes-scapularis_M_Drag_2019-05-31	OL704337
NYSDOH	PV217-19095-165_LII_North-Blenheim_NY_USA_Ixodes-scapularis_M_Drag_2019-05-30	OL704338
NYSDOH	PV218-13CD01-002_LII_Copake_NY_USA_Ixodes-scapularis_M_Deer_2013-11-16	OL704339
NYSDOH	PV222-14021-346_LII_Clermont_NY_USA_Ixodes-scapularis_F_Drag_2014-11-25	OL704340
NYSDOH	PV223-14021-358_LII_Clermont_NY_USA_Ixodes-scapularis_M_Drag_2014-11-25	OL704341
NYSDOH	PV224-14021-472_LII_Chatham_NY_USA_Ixodes-scapularis_M_Drag_2014-11-25	OL704342
NYSDOH	PV227-14087-111_LII_Montebello_NY_USA_Ixodes-scapularis_M_Drag_2014-11-04	OL704343
NYSDOH	PV228-14105-140_LII_Mamakating_NY_USA_Ixodes-scapularis_M_Drag_2014-10-28	OL704344
NYSDOH	PV229-17091-15-003_LII_Stillwater_NY_USA_Ixodes-scapularis_M_Deer_2017-11-18	OL704345
NYSDOH	PV230-17105-109_LII_Mamakating_NY_USA_Ixodes-scapularis_F_Drag_2017-10-27	OL704346
NYSDOH	PV231-17119-29-002_LII_Pound-Ridge_NY_USA_Ixodes-scapularis_M_Deer_2017-11-13	OL704347
NYSDOH	PV232-18103-167-010_LII_Shelter-Island_NY_USA_Ixodes-scapularis_F_Deer_2018-11-01	OL704348
NYSDOH	PV233-18103-168-007_LII_Shelter-Island_NY_USA_Ixodes-scapularis_Unknown_Deer_2018-11-01	OL704349
NYSDOH	PV234-18071-054_LII_Wallkill_NY_USA_Ixodes-scapularis_N_Drag_2018-11-06	OL704350
NYSDOH	PV235-18079-053_LII_Brewster_NY_USA_Ixodes-scapularis_N_Drag_2018-05-31	OL704351
NYSDOH	PV236-18087-055_LII_Montebello_NY_USA_Ixodes-scapularis_N_Drag_2018-06-18	OL704352
NYSDOH	PV237-18091-128_LII_Saratoga-Springs_NY_USA_Ixodes-scapularis_M_Drag_2018-06-27	OL704353
NYSDOH	PV239-18103-058_LII_Smithtown_NY_USA_Ixodes-scapularis_F_Drag_2018-02-27	OL704354
NYSDOH	PV240-18103-1315_LII_Huntington_NY_USA_Ixodes-scapularis_N_Drag_2018-06-07	OL704355
NYSDOH	PV241-18103-1419_LII_Smithtown_NY_USA_Ixodes-scapularis_N_Drag_2018-06-06	OL704356
NYSDOH	PV242-18103-281_LII_East-Hampton_NY_USA_Ixodes-scapularis_N_Drag_2018-06-19	OL704357
NYSDOH	PV243-17021-304_LII_Greenport_NY_USA_Ixodes-scapularis_F_Drag_2017-11-01	OL704358
NYSDOH	PV244-17021-341_LII_Taghkanic_NY_USA_Ixodes-scapularis_F_Drag_2017-11-01	OL704359
NYSDOH	PV245-17091-11-001_LII_Stillwater_NY_USA_Ixodes-scapularis_M_Deer_2017-11-18	OL704360
NYSDOH	PV246-17091-23-002_LII_Saratoga_NY_USA_Ixodes-scapularis_M_Deer_2017-11-18	OL704361
NYSDOH	PV247-17091-24-003_LII_Ballston-Spa_NY_USA_Ixodes-scapularis_M_Deer_2017-11-18	OL704362
NYSDOH	PV248-17091-27-004_LII_Clifton-Park_NY_USA_Ixodes-scapularis_M_Deer_2017-11-19	OL704363
NYSDOH	PV249-17091-391_LII_Wilton_NY_USA_Ixodes-scapularis_F_Drag_2017-10-27	OL704364
NYSDOH	PV250-17091-457_LII_Saratoga-Springs_NY_USA_Ixodes-scapularis_F_Drag_2017-11-09	OL704365
NYSDOH	PV251-17091-474_LII_Greenfield_NY_USA_Ixodes-scapularis_F_Drag_2017-11-09	OL704366
NYSDOH	PV252-17091-500_LII_Northumberland_NY_USA_Ixodes-scapularis_M_Drag_2017-11-15	OL704367
NYSDOH	PV253-17091-536_LII_Stillwater_NY_USA_Ixodes-scapularis_M_Drag_2017-11-15	OL704368
NYSDOH	PV254-17091-654_LII_Malta_NY_USA_Ixodes-scapularis_F_Drag_2017-11-09	OL704369
NYSDOH	PV255-17091-658_LII_Malta_NY_USA_Ixodes-scapularis_M_Drag_2017-11-09	OL704370
NYSDOH	PV256-17091-660_LII_Malta_NY_USA_Ixodes-scapularis_M_Drag_2017-11-09	OL704371
NYSDOH	PV257-17103-1037_LII_Islip_NY_USA_Ixodes-scapularis_F_Drag_2017-11-21	OL704372
NYSDOH	PV258-17103-1045_LII_Huntington_NY_USA_Ixodes-scapularis_M_Drag_2017-10-27	OL704373
NYSDOH	PV259-17103-973_LII_East-Hampton_NY_USA_Ixodes-scapularis_M_Drag_2017-11-15	OL704374
NYSDOH	PV260-17115-194_LII_Greenwich_NY_USA_Ixodes-scapularis_M_Drag_2017-10-27	OL704375
NYSDOH	PV261-19001-855_LII_Guilderland_NY_USA_Ixodes-scapularis_F_Drag_2019-10-15	OL704376
NYSDOH	PV262-19001-866_LII_Guilderland_NY_USA_Ixodes-scapularis_F_Drag_2019-10-15	OL704377
NYSDOH	PV263-19001-899_LII_Guilderland_NY_USA_Ixodes-scapularis_M_Drag_2019-10-15	OL704378
NYSDOH	PV264-19021-783_LII_Copake_NY_USA_Ixodes-scapularis_F_Drag_2019-11-06	OL704379
NYSDOH	PV265-19021-794_LII_Copake_NY_USA_Ixodes-scapularis_F_Drag_2019-11-06	OL704380
NYSDOH	PV266-19039-373_LII_Windham_NY_USA_Ixodes-scapularis_M_Drag_2019-10-25	OL704381
NYSDOH	PV267-19039-497_LII_Cairo_NY_USA_Ixodes-scapularis_M_Drag_2019-10-25	OL704382
NYSDOH	PV268-19083-510_LII_Schodack_NY_USA_Ixodes-scapularis_F_Drag_2019-11-05	OL704383
NYSDOH	PV269-19083-516_LII_Schodack_NY_USA_Ixodes-scapularis_F_Drag_2019-11-05	OL704384

NYSDOH	PV270-19091-625_LII_Malta_NY_USA_Ixodes-scapularis_F_Drag_2019-10-10	OL704385
NYSDOH	PV271-19093-494_LII_Glenville_NY_USA_Ixodes-scapularis_F_Drag_2019-11-04	OL704386
NYSDOH	PV272-19065-058_LI_Verona_NY_USA_Ixodes-scapularis_M_Drag_2019-11-04	OL704387
NYSDOH	PV273-19065-059_LI_Verona_NY_USA_Ixodes-scapularis_F_Drag_2019-11-04	OL704388
NYSDOH	PV274-19021-02-002_LII_Ancram_NY_USA_Ixodes-scapularis_M_Deer_2019-11-16	OL704389
NYSDOH	PV275-19021-03-002_LII_North-East_NY_USA_Ixodes-scapularis_M_Deer_2019-11-16	OL704390
NYSDOH	PV276-19021-09-001_LII_Taghkanic_NY_USA_Ixodes-scapularis_M_Deer_2019-11-16	OL704391
NYSDOH	PV277-19091-04-001_LII_Ballston_NY_USA_Ixodes-scapularis_M_Deer_2019-11-16	OL704392
NYSDOH	PV278-19091-08-002_LII_Stillwater_NY_USA_Ixodes-scapularis_M_Deer_2019-11-16	OL704393
NYSDOH	PV279-19091-11-001_LII_Greenwich_NY_USA_Ixodes-scapularis_M_Deer_2019-11-16	OL704394

Supplementary Table 4: Comparison of lineage dispersal velocities estimated for different data sets of viral genomes. The table comes from the study of Klitting et al. (2021)[75] and has been completed with the estimate obtained from the continuous phylogeographic reconstruction of POWV lineages in Northeastern USA. For each data set, we report both the posterior median estimate and the 95% HPD interval.

Data set	Weighted lineage dispersal velocity	Num. of samples	Reference
Nova virus (moles), Belgium	0.3 km/year [0.3, 0.4]	100	Laenen et al. (2016)
Lassa virus, segment S, Africa	0.8 km/year [0.7, 1.0]	254	Klitting et al. (2021)
Lassa virus, segment L, Africa	1.0 km/year [0.9, 1.0]	410	Klitting et al. (2021)
Powassan virus, USA	3.1 km/year [2.6, 3.8]	319	(present study)
Rabies virus (skunks), USA	9.4 km/year [8.3, 10.6]	241	Kuzmina et al. (2013)
Rabies virus (raccoons), USA	11.8 km/year [9.6, 13.3]	47	Biek et al. (2007)
Rabies virus (bats), eastern Brazil	12.5 km/year [7.8, 20.3]	41	Vieira et al. (2013)
Rabies virus (dogs), northern Africa	16.8 km/year [14.0, 19.7]	250	Talbi et al. (2010)
Rabies virus (bats), Peru	17.7 km/year [14.6, 21.1]	260	Streicker et al. (2016)
Rabies virus (mainly dogs), Iran	18.1 km/year [16.3, 20.8]	105	Dellicour et al. (2019)
Rabies virus (bats), Argentina	34.7 km/year [28.1, 41.6]	131	Torres et al. (2014)
H5N1 virus, Mekong region	149.0 km/year [115.9, 170.2]	320	Dellicour et al. (2020a)
West Nile virus, North America	165.0 km/year [158.0, 169.2]	801	Dellicour et al. (2020b)
Yellow fever virus, Brazil	169.4 km/year [131.7, 214.4]	99	Hill et al. (2020)
Porcine deltacoronavirus, China	184.7 km/year [134.7, 234.4]	97	He et al. (2020)
Ebola virus, West Africa	598.1 km/year [556.4, 635.3]	722	Dellicour et al. (2020)

Supplementary Table 5: Impact of several environmental factors on the dispersal location of POWV lineages. We report Bayes factor (BF) support for the association between environmental values and tree node locations. The results are based on 1,000 posterior trees obtained by spatially-explicit phylogeographic inference. Following Kass & Raftery (1995), we consider a BF value >20 as strong support for a significant correlation between the environmental distances and dispersal durations (in bold). "ENM" refers to ecological niche modeling.

Environmental factor	Tendency of viral lineages to avoid circulating within specific environmental conditions	Tendency of viral lineages to preferentially circulate within specific environmental conditions
Elevation	**>99**	0.0
Forest areas	9.6	0.1
Croplands	0.2	5.9
Urban areas	0.4	2.8
Annual mean Temperature	0.1	13.3
Annual precipitation	8.7	0.1

Supplementary Table 6: Impact of several environmental factors on the dispersal velocity of POWV lineages. The results are based on 1,000 posterior trees obtained by spatially-explicit phylogeographic inference. "C" and "R" indicate if the considered environmental raster was considered as a conductance

("C") or resistance factor ("R"), and *k* is the rescaling parameter used to transform the initial raster (see the text for further details). For regression coefficients and *Q* values we report both the median estimate and the 95% HPD interval. The Bayes factor (BF) supports are only reported when p(*Q* > 0) is at least 90%. Following Kass & Raftery (1995), we consider a BF value >20 as strong support for a significant correlation between the environmental distances and dispersal durations (in bold).

Path model	Environmental factor	*k*	Regression coefficient	*Q* statistic	p(*Q* > 0)	BF
Least-cost algorithm	elevation (C)	10	0.091 [0.033, 0.225]	0.002 [-0.017, 0.045]	0.558	-
		100	0.074 [0.020, 0.230]	-0.013 [-0.058, 0.065]	0.302	-
		1000	0.061 [0.013, 0.222]	-0.024 [-0.079, 0.066]	0.239	-
	elevation (R)	10	0.085 [0.041, 0.162]	-0.003 [-0.037, 0.012]	0.362	-
		100	0.073 [0.041, 0.120]	-0.014 [-0.082, 0.016]	0.211	-
		1000	0.064 [0.035, 0.101]	-0.023 [-0.106, 0.012]	0.132	-
	forest areas (C)	10	0.080 [0.023, 0.236]	-0.009 [-0.043, 0.070]	0.369	-
		100	0.048 [0.006, 0.213]	-0.036 [-0.087, 0.051]	0.140	-
		1000	0.022 [0.000, 0.166]	-0.056 [-0.12, 0.020]	0.055	-
	forest areas (R)	10	0.075 [0.037, 0.161]	-0.012 [-0.058, 0.013]	0.215	-
		100	0.070 [0.035, 0.153]	-0.016 [-0.072, 0.015]	0.201	-
		1000	0.070 [0.035, 0.152]	-0.016 [-0.073, 0.015]	0.200	-
	croplands (C)	10	0.086 [0.033, 0.203]	-0.002 [-0.018, 0.027]	0.400	-
		100	0.090 [0.034, 0.228]	0.001 [-0.033, 0.071]	0.518	-
		1000	0.080 [0.028, 0.213]	-0.005 [-0.058, 0.067]	0.434	-
	croplands (R)	10	0.098 [0.046, 0.198]	0.009 [-0.012, 0.032]	0.834	-
		100	0.057 [0.023, 0.152]	-0.028 [-0.095, 0.021]	0.134	-
		1000	0.034 [0.010, 0.118]	-0.050 [-0.128, 0.003]	0.035	-
	urban areas (C)	10	0.078 [0.041, 0.151]	-0.008 [-0.059, 0.017]	0.302	-
		100	0.051 [0.028, 0.093]	-0.035 [-0.113, 0.005]	0.050	-
		1000	0.035 [0.018, 0.064]	-0.052 [-0.14, -0.008]	0.006	-
	urban areas (R)	10	0.079 [0.020, 0.239]	-0.009 [-0.049, 0.079]	0.386	-
		100	0.046 [0.003, 0.194]	-0.037 [-0.102, 0.048]	0.170	-
		1000	0.040 [0.001, 0.184]	-0.042 [-0.109, 0.042]	0.131	-
	water areas (C)	10	0.066 [0.036, 0.114]	-0.021 [-0.108, 0.025]	0.204	-
		100	0.062 [0.033, 0.112]	-0.025 [-0.113, 0.024]	0.194	-
		1000	0.060 [0.031, 0.109]	-0.026 [-0.114, 0.024]	0.179	-
	water areas (R)	10	0.122 [0.056, 0.249]	0.031 [-0.031, 0.117]	0.797	-
		100	0.114 [0.022, 0.238]	0.024 [-0.093, 0.142]	0.642	-
		1000	0.087 [0.007, 0.204]	-0.004 [-0.122, 0.118]	0.480	-
	annual mean temperature (C)	10	0.096 [0.043, 0.178]	0.002 [-0.054, 0.073]	0.521	-
		100	0.095 [0.043, 0.175]	0.001 [-0.056, 0.070]	0.514	-
		1000	0.095 [0.043, 0.175]	0.001 [-0.056, 0.069]	0.513	-
	annual mean temperature (R)	10	0.112 [0.046, 0.222]	0.020 [-0.042, 0.104]	0.681	-
		100	0.113 [0.046, 0.226]	0.021 [-0.041, 0.106]	0.690	-
		1000	0.114 [0.046, 0.227]	0.021 [-0.041, 0.106]	0.692	-
	annual precipitation (C)	10	0.103 [0.046, 0.198]	0.011 [-0.049, 0.085]	0.604	-
		100	0.104 [0.046, 0.198]	0.011 [-0.049, 0.085]	0.606	-
		1000	0.104 [0.046, 0.198]	0.011 [-0.049, 0.084]	0.606	-
	annual precipitation (R)	10	0.104 [0.045, 0.203]	0.012 [-0.047, 0.088]	0.611	-
		100	0.104 [0.045, 0.203]	0.012 [-0.047, 0.088]	0.613	-
		1000	0.104 [0.045, 0.203]	0.012 [-0.047, 0.088]	0.613	-
Circuitscape algorithm	elevation (C)	10	0.061 [0.011, 0.232]	-0.023 [-0.048, -0.010]	0.000	-
		100	0.035 [0.003, 0.189]	-0.045 [-0.101, -0.018]	0.000	-
		1000	0.026 [0.001, 0.169]	-0.053 [-0.126, -0.019]	0.000	-
	elevation (R)	10	0.120 [0.046, 0.288]	0.029 [-0.008, 0.051]	0.958	4.0
		100	0.131 [0.071, 0.233]	0.044 [-0.078, 0.097]	0.812	-
		1000	0.125 [0.071, 0.210]	0.036 [-0.106, 0.099]	0.744	-
	forest areas (C)	10	0.038 [0.003, 0.204]	-0.042 [-0.101, -0.017]	0.000	-
		100	0.020 [0.000, 0.164]	-0.058 [-0.140, -0.021]	0.000	-
		1000	0.011 [0.000, 0.148]	-0.067 [-0.149, -0.022]	0.000	-
	forest areas (R)	10	0.109 [0.053, 0.228]	0.022 [-0.082, 0.064]	0.758	-

	100	0.103 [0.052, 0.199]	0.015 [-0.119, 0.075]	0.652	-
	1000	0.101 [0.052, 0.194]	0.013 [-0.124, 0.077]	0.633	-
croplands (C)	10	0.091 [0.027, 0.255]	0.003 [-0.044, 0.048]	0.555	-
	100	0.074 [0.019, 0.225]	-0.01 [-0.094, 0.064]	0.383	-
	1000	0.060 [0.011, 0.197]	-0.021 [-0.123, 0.059]	0.281	-
croplands (R)	10	0.050 [0.008, 0.171]	-0.034 [-0.117, -0.002]	0.017	-
	100	0.020 [0.002, 0.121]	-0.060 [-0.205, -0.017]	0.001	-
	1000	0.014 [0.001, 0.115]	-0.064 [-0.218, -0.018]	0.001	-
urban areas (C)	10	0.088 [0.032, 0.212]	0.002 [-0.101, 0.044]	0.529	-
	100	0.066 [0.030, 0.164]	-0.018 [-0.166, 0.049]	0.329	-
	1000	0.043 [0.017, 0.130]	-0.040 [-0.198, 0.033]	0.179	-
urban areas (R)	10	0.054 [0.006, 0.208]	-0.025 [-0.103, 0.01]	0.085	-
	100	0.042 [0.002, 0.182]	-0.036 [-0.130, 0.005]	0.045	-
	1000	0.040 [0.001, 0.178]	-0.037 [-0.136, 0.004]	0.041	-
water areas (C)	10	0.085 [0.046, 0.153]	0.002 [-0.175, 0.087]	0.516	-
	100	0.059 [0.028, 0.123]	-0.024 [-0.201, 0.061]	0.330	-
	1000	0.050 [0.023, 0.113]	-0.033 [-0.208, 0.05]	0.260	-
water areas (R)	10	0.114 [0.044, 0.215]	0.023 [-0.151, 0.134]	0.653	-
	100	0.061 [0.009, 0.151]	-0.028 [-0.203, 0.089]	0.311	-
	1000	0.054 [0.006, 0.141]	-0.034 [-0.209, 0.082]	0.268	-
annual mean temperature (C)	10	0.163 [0.074, 0.283]	0.068 [-0.071, 0.184]	0.858	-
	100	0.163 [0.075, 0.282]	0.068 [-0.074, 0.182]	0.858	-
	1000	0.163 [0.075, 0.282]	0.068 [-0.074, 0.182]	0.858	-
annual mean temperature (R)	10	0.159 [0.060, 0.303]	0.062 [-0.068, 0.184]	0.853	-
	100	0.158 [0.059, 0.302]	0.061 [-0.068, 0.183]	0.851	-
	1000	0.158 [0.058, 0.302]	0.061 [-0.068, 0.183]	0.850	-
annual precipitation (C)	10	0.165 [0.069, 0.296]	0.069 [-0.065, 0.185]	0.863	-
	100	0.165 [0.070, 0.296]	0.068 [-0.065, 0.185]	0.863	-
	1000	0.165 [0.069, 0.296]	0.068 [-0.065, 0.185]	0.863	-
annual precipitation (R)	10	0.164 [0.066, 0.297]	0.069 [-0.065, 0.190]	0.859	-
	100	0.163 [0.065, 0.297]	0.069 [-0.065, 0.190]	0.859	-
	1000	0.163 [0.065, 0.297]	0.069 [-0.065, 0.190]	0.859	-

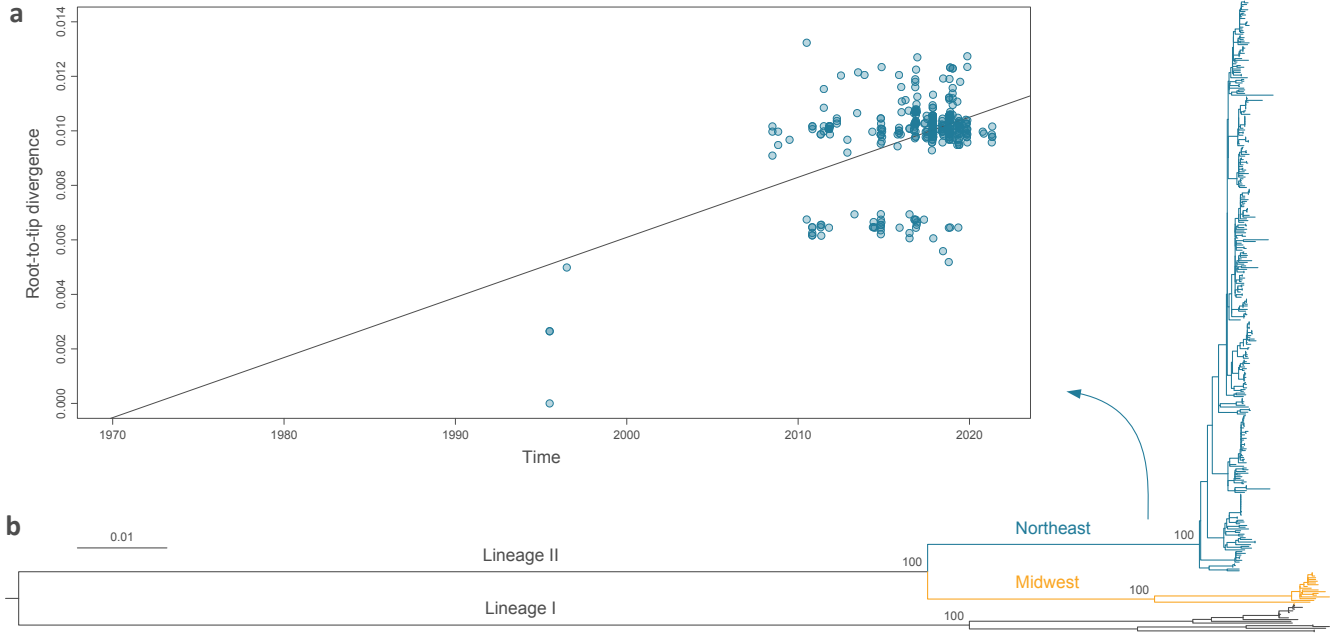
a
Root-to-tip divergence
0.000
0.002
0.004
0.006
0.008
0.010
0.012
0.014
1970
1980
1990
2000
2010
2020
Time
b
0.01
Lineage II
Lineage I
Northeast
Midwest
100
100
100
100

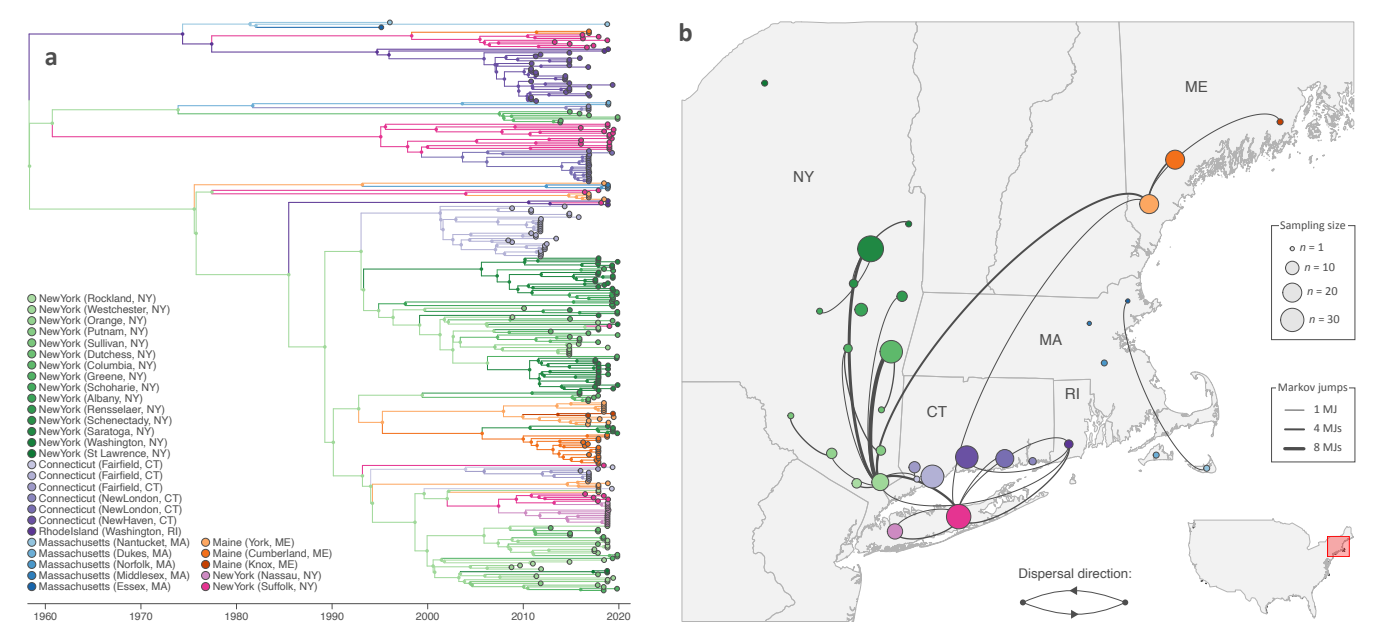
a
NewYork (Rockland, NY)
NewYork (Westchester, NY)
NewYork (Orange, NY)
NewYork (Putnam, NY)
NewYork (Sullivan, NY)
NewYork (Dutchess, NY)
NewYork (Columbia, NY)
NewYork (Greene, NY)
NewYork (Schoharie, NY)
NewYork (Albany, NY)
NewYork (Rensselaer, NY)
NewYork (Schenectady, NY)
NewYork (Saratoga, NY)
NewYork (Washington, NY)
NewYork (St Lawrence, NY)
Connecticut (Fairfield, CT)
Connecticut (Fairfield, CT)
Connecticut (Fairfield, CT)
Connecticut (NewLondon, CT)
Connecticut (NewLondon, CT)
Connecticut (NewHaven, CT)
RhodeIsland (Washington, RI)
Massachusetts (Nantucket, MA)
Massachusetts (Dukes, MA)
Massachusetts (Norfolk, MA)
Massachusetts (Middlesex, MA)
Massachusetts (Essex, MA)
Maine (York, ME)
Maine (Cumberland, ME)
Maine (Knox, ME)
NewYork (Nassau, NY)
NewYork (Suffolk, NY)
1960
1970
1980
1990
2000
2010
2020
b
NY
ME
MA
RI
CT
Sampling size
n = 1
n = 10
n = 20
n = 30
Markov jumps
1 MJ
4 MJs
8 MJs
Dispersal direction:

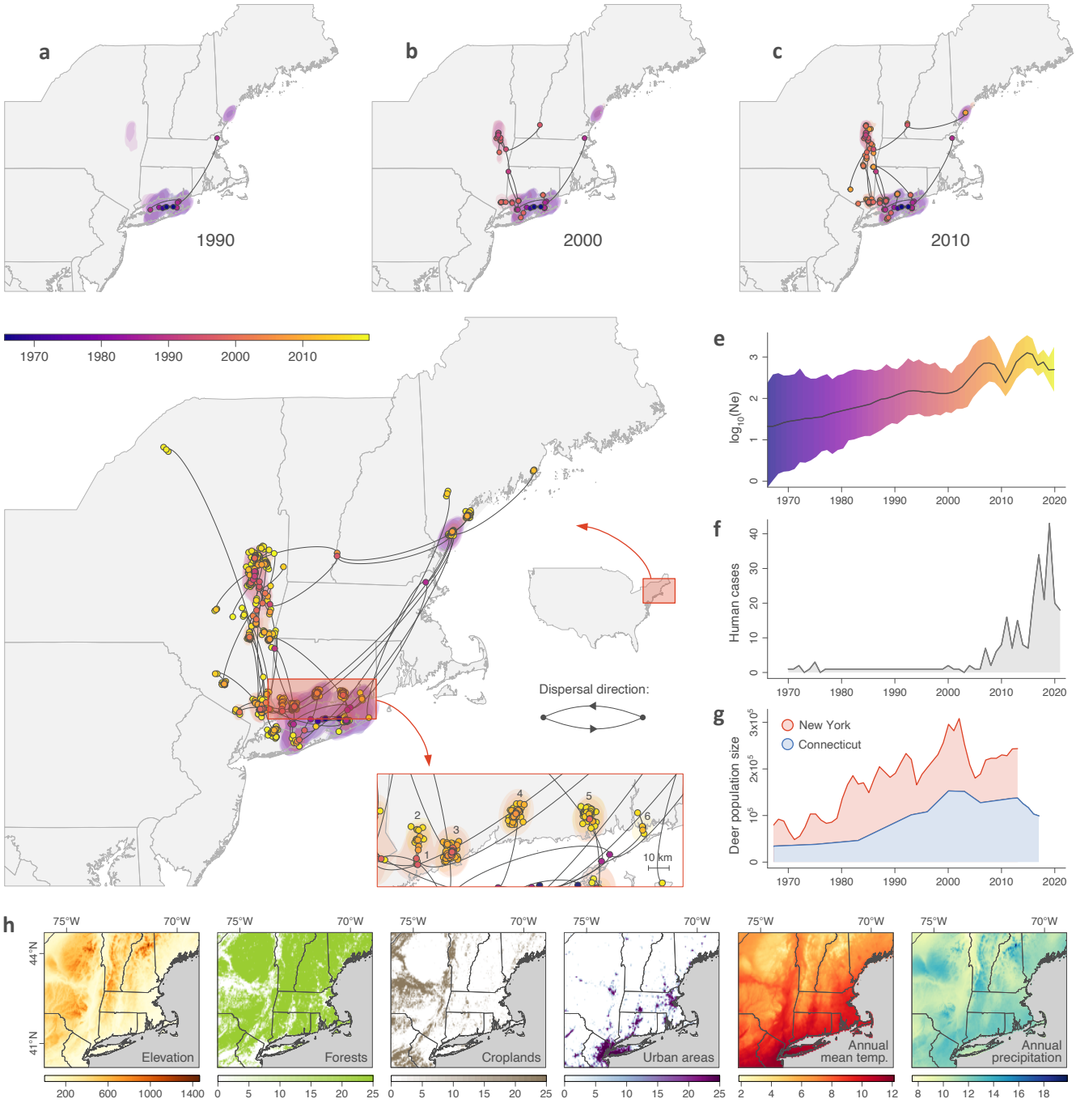
a
1990
b
2000
c
2010
1970
1980
1990
2000
2010
Dispersal direction:
1
2
3
4
5
6
10 km
e
log10(Ne)
f
Human cases
g
Deer population size
New York
Connecticut
h
75°W
70°W
44°N
41°N
Elevation
Forests
Croplands
Urban areas
Annual mean temp.
Annual precipitation

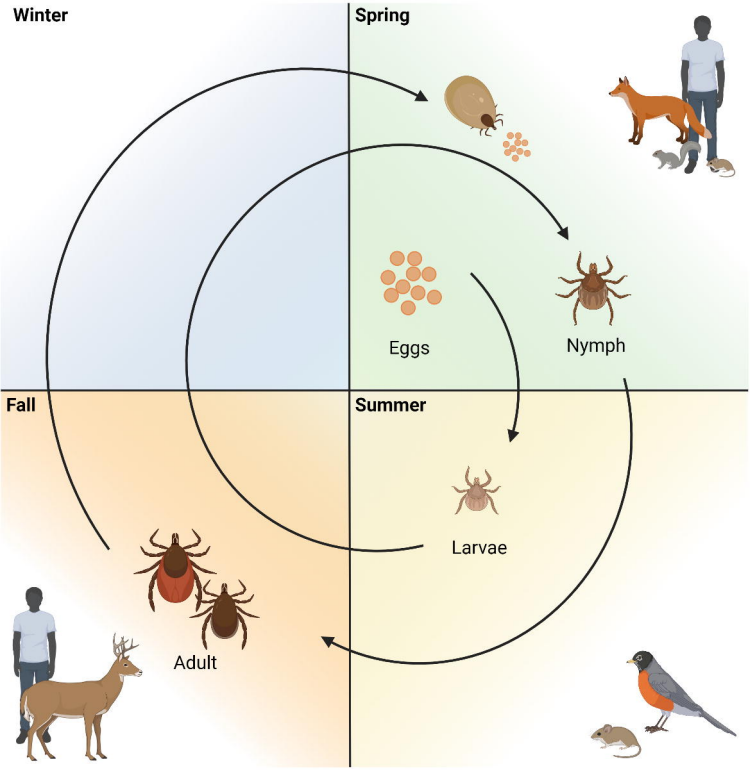

Hypothesis 1: Minor role for vertical transmission

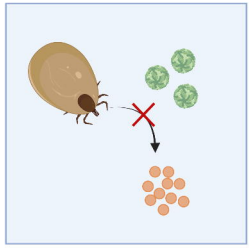

Hypothesis 2: Major role for backward transmission from nymphs to larvae